IEEE Access
Multidisciplinary | Rapid Review | Open Access Journal

Received April 29, 2020, accepted May 11, 2020, date of publication May 27, 2020, date of current version June 9, 2020.

*Digital Object Identifier 10.1109/ACCESS.2020.2998064*

# Generalized Framework for Hybrid Analog/Digital Signal Processing in Massive and Ultra-Massive-MIMO Systems

**ALIREZA MORSALI[1], (Graduate Student Member, IEEE), AFSHIN HAGHIGHAT[2], (Senior Member, IEEE), AND BENOIT CHAMPAGNE[1], (Senior Member, IEEE)**

[1]Department of Electrical and Computer Engineering, McGill University, Montreal, QC H3A 0G4, Canada
[2]InterDigital Canada, Inc., Montreal, QC H3A 3G4, Canada

Corresponding author: Alireza Morsali (alireza.morsali@mail.mcgill.ca)

This work was supported in part by the Natural Sciences and Engineering Research Council of Canada (NSERC), and in part by the InterDigital Canada, Inc.

**ABSTRACT** The conventional fully-digital implementation of massive-MIMO systems is not efficient due to the large required number of radio-frequency (RF) chains. To address this issue, hybrid analog/digital (A/D) beamforming was proposed and to date remains a topic of ongoing research. In this paper, we explore the hybrid A/D structure as a general framework for signal processing in massive and ultra-massive-MIMO systems. To exploit the full potential of the analog domain, we first focus on the analog signal processing (ASP) network. We investigate a mathematical representation suitable for any arbitrarily connected feed-forward ASP network comprised of the common RF hardware elements in the context of hybrid A/D systems, i.e., phase-shifter and power-divider/combiner. A novel ASP structure is then proposed which is not bound to the unit modulus constraint, thereby facilitating the hybrid A/D systems design. We then study MIMO transmitter and receiver designs to exploit the full potential of digital processing as well. It is shown that replacing the linear transformation in the digital domain with a generic mapping can improve the system performance. In some cases, the performance of optimal fully-digital MIMO systems can be achieved without extra calculations compared to sub-optimal hybrid A/D techniques. An optimization model based on the proposed structure is presented that can be used for hybrid A/D system design. Specifically, precoding and combining designs under different conditions are discussed as examples. Finally, simulation results are presented which illustrate the superiority of the proposed architecture to the conventional hybrid designs for massive-MIMO systems.

**INDEX TERMS** Hybrid beamforming, hybrid analog and digital signal processing, ultra massive MIMO, massive MIMO, precoding, combining, beamforming.

## I. INTRODUCTION

Massive-multiple-input multiple-output (MIMO) and (ultra-massive) UM-MIMO systems operating in millimeter wave (mmW)/Terahertz (THz) bands are the prime candidates for fifth generation (5G) and beyond 5G cellular networks [1]–[4]. In fact, base-stations (BS) with 64 antennas have been recently deployed for commercial use in some countries [5]. Moreover, an extensive theory for massive MIMO has been developed in recent years, including capacity and spectral efficiency analysis, system design for high energy efficiency, pilot contamination, etc. However, implementation of such systems faces many technical difficulties, and to this day remains very challenging and costly [6], [7]. In conventional fully-digital (FD) MIMO systems, each antenna element requires a dedicated radio frequency (RF) chain. The direct FD implementation for massive-MIMO/UM-MIMO systems, however, is not practical and efficient due to the ensuing high production costs and more importantly, huge power consumption.

Hybrid analog/digital (A/D) signal processing (HSP) is an effective approach to overcome this problem by cascading

The associate editor coordinating the review of this manuscript and approving it for publication was Miguel López-Benítez.

an analog signal processing (ASP) network to the baseband digital signal processor [8], [9]. While in conventional FD MIMO transmitters [10]–[12], each antenna element is directly controlled by the digital processor, in an HSP-based transmitter, the digital processor generates a low-dimensional RF signal vector, whose size is then increased by analog circuitry for driving the large-scale antenna array. Similarly, in an HSP-based receiver, the size of the large-dimensional vector of antenna signals is reduced by an ASP network, whose outputs are then converted to the digital domain for baseband processing by means of RF chains.

There are practical constraints in the implementation and design of ASP networks and only a few types of RF components are commonly used in practice. Specifically, the power-divider (splitter), power-combiner (adder), and phase-shifter are the key analog components of the ASP design [13]–[22]. In the existing hybrid beamforming structures, due to the particular configuration of the aforementioned analog components, a constant modulus constraint is imposed on the analog beamformer weights which turns the beamforming design into an intractable non-convex optimization problem [13], [14].

### A. RELATED WORKS

In one of the earliest works in this field [8], it is shown that for a single data stream, two RF chains are required to achieve the performance of a FD combiner. This technique was extended to multiple stream beamforming (i.e., precoding/combining) where the required number of RF chains must be twice the number of the data streams [14], [15]. In [23], [24], we proposed a single RF chain FD precoding realization. Many researchers, however, focused on developing the hybrid beamformers directly by solving non-convex design optimization problems [13]–[21].

In [13], the beamformer design was formulated as the minimization of the Euclidean distance between the hybrid beamformer and the FD one. Then, by taking into account the sparse characteristics of the mmWave channels, compressed sensing (CS) techniques were presented to solve the underlying optimization problems. The same authors, extended their results to wide-band systems in [25]. This approach was later used in [21] and [16] where in the latter, manifold optimization algorithms as well as other low-complexity algorithms were used for hybrid beamformer design. Directly tackling the non-convex design optimization problems was attempted in [14] where the authors took advantage of orthogonalization techniques and exploited the sparsity of the channel for designing the hybrid beamformers. These results were then extended to wide-band systems in [26]. In [27], the Gram-Schmidt method was used specifically in uplink multi-user (MU) scenario for designing robust low-complexity beamformers. Robust beamformers for single-user (SU) were studied in [18] by minimizing the sum-power of interfering signals. In [17], a simple non-iterative algorithm was proposed for hybrid regularized channel diagolnalization and in [27] the mean square error (MSE) was chosen as the cost function for designing the hybrid beamformers.

The majority of the above works consider a fully-connected architecture, i.e., each RF chain is connected to all of the antenna elements. Alternatively, in a sub-connected architecture, only a subset of RF chains are connected to each antenna [16], [28], [29]. Recently, a dynamic sub-connected hybrid architecture has been proposed in [29] for multi-user equalization in wideband millimeter-wave massive MIMO systems, based on the minimization of the sum of MSE over multiple subcarriers. Although sub-connected designs require less RF components, fully-connected ones can achieve a superior performance in theory. Hence, in this study, we investigate properties of fully-connected ASP networks.

### B. CONTRIBUTIONS AND PAPER ORGANIZATION

In this paper, our goal is to investigate and exploit the full potential of HSP in massive-MIMO systems. Aiming at this challenge, we can summarize our contributions as follows

- We first explore the degrees of freedom in the analog domain by developing a compact mathematical representation for any given feed-forward ASP network with arbitrary connections of any number of RF components, i.e., phase-shifters, power dividers and power combiners.
- Based on the above generalization, a simple and novel ASP architecture is conceived out of the above RF components, which is not bound to the constant modulus constraint. Removing this constraint facilitates system design as non-convex optimizations are difficult to solve and global optimality of the solutions cannot usually be guaranteed.
- The transmitter and receiver sides are then studied separately by exploiting the newly proposed ASP architecture and generalizing generalizing the digital processing. Specifically, the optimization problem for the HSP beamformer is reformulated within the new representation framework, which facilitates its solution under a variety of constraints and requirements for the massive MIMO system.
- The realization of optimal FD by HSP and the problem of RF chain minimization are presented as guideline examples to illustrate potential applications of the proposed theoretical framework.
- Simulation results of optimal beamformer designs with the proposed architecture are finally presented. The results demonstrate that the new designs can achieve the same performance as the corresponding optimal FD system and hence, outperform recently published hybrid beamformer designs.

The paper is organized as follows. In Section II, the system model is explained. We then study ASP networks in Section III followed by transmitter and receiver design in Sections IV. Simulation results are presented in Section V. We then conclude the paper in Section VI.

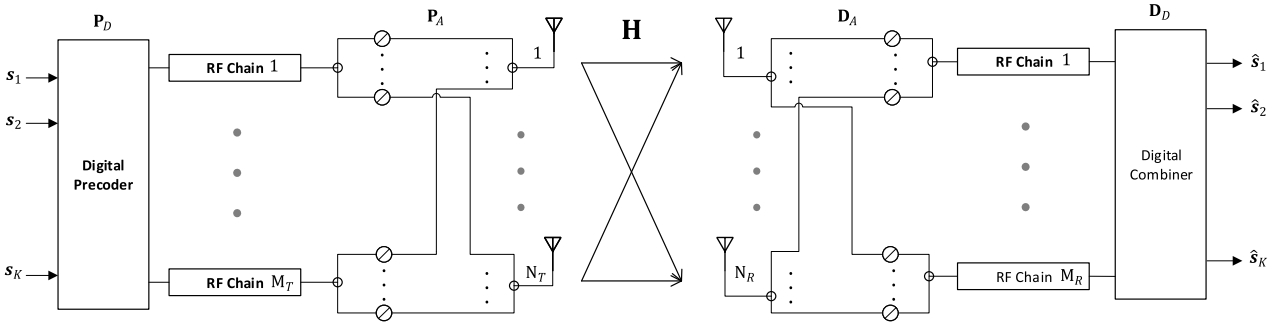


**FIGURE 1.** Conventional HSP architecture for single user massive-MIMO system.

*Notations:* Throughout this paper we use bold capital and lowercase letters to represent matrices and vectors, respectively. Superscripts $(.)^H$, $(.)^t$, and $(.)^*$ indicate Hermitian, transpose, and complex conjugations, respectively. $\mathbf{I}_n$ denotes an identity matrix of size $n \times n$ while $\mathbf{0}_{n\times m}$ denotes an all zero matrix with size $n \times m$ and $\mathbf{1}_n$ is an all one column vector of size $\eta$. The element on the $p^{th}$ row and the $q^{th}$ column of matrix $\mathbf{A}$ is denoted by $A_{p,q}$ while the $p^{th}$ element of vector $\mathbf{x}$ is denoted by $x_p$. $\mathrm{Tr}(\mathbf{A})$ and $\|\mathbf{A}\|_F$ denote trace and Frobenius norm of matrix $\mathbf{A}$, respectively. $\mathbf{A} = \mathrm{bd}(\mathbf{A}_1, \mathbf{A}_2, \ldots, \mathbf{A}_n)$ represents a block-diagonal matrix, in which $\mathbf{A}_1, \mathbf{A}_2, \ldots, \mathbf{A}_n$ are the diagonal blocks of $\mathbf{A}$. The Kronecker product is denoted by $\otimes$. By $\mathbf{x}_1 \overset{\pi}{=} \mathbf{x}_2$, it is meant that there exist a permutation matrix $\mathbf{P}_\pi$ such that $\mathbf{x}_1 = \mathbf{P}_\pi \mathbf{x}_2$. The greatest (least) integer less (greater) than or equal to $x$ is denoted by $\lfloor x \rfloor$ ($\lceil x \rceil$). Moreover, $x = a \bmod n$ denotes the remainder of the division of $a$ by $n$. The absolute value and phase of a complex number $z = |z| \exp(j\angle z)$ are denoted by $|z|$ and $\angle z$. $\mathbb{C}$ stands for the complex field. A complex circular Gaussian random vector $\mathbf{x} \in \mathbb{C}^n$ with mean vector $\mathbf{m} = \mathbb{E}\{\mathbf{x}\}$ and covariance matrix $\mathbf{R} = \mathbb{E}\{\mathbf{x}\mathbf{x}^H\}$ is denoted by $\mathcal{CN}(\mathbf{m}, \mathbf{R})$ where $\mathbb{E}\{\}$ stands for expectation.

## II. SYSTEM MODEL

We consider a generic point-to-point massive-MIMO system where the transmitter and receiver are equipped with $N_T$ and $N_R$ antennas as well as $M_T$ and $M_R$ RF chains, respectively. In the context of HSP, due to practical constraints, it is further assumed that $M_T \ll N_T$ and $M_R \ll N_R$.

### A. CONVENTIONAL HYBRID BEAMFORMING

Fig. 1 illustrates a point-to-point massive-MIMO system with conventional hybrid beamforming implemented at both ends. The transmitted signal over one symbol duration $T_s$ can be formulated as

$$\mathbf{x} = \sqrt{\rho}\,\mathbf{P}_A\mathbf{P}_D\mathbf{s}, \tag{1}$$

where $\mathbf{s} = [s_1, s_2, \ldots, s_K]^t$ is the symbol vector with zero-mean random information symbols $s_k$'s taken from a discrete constellation $\mathscr{A}$ (such as M-QAM or M-PSK), normalized such that $\mathbb{E}\{\mathbf{s}\mathbf{s}^H\} = \mathbf{I}_K$ and, $\rho$ is the average transmit power. Matrices $\mathbf{P}_D \in \mathbb{C}^{M_T\times K}$ and $\mathbf{P}_A \in \mathbb{U}^{N_T\times M_T}$ are the digital and analog precoders, respectively, where $\mathbb{U} = \{z \in \mathbb{C}: |z| = 1\}$ and for normalization purposes, it is further assumed that $\|\mathbf{P}_A\mathbf{P}_D\|_F^2 = 1$.

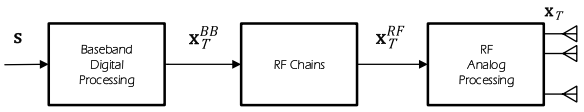


**FIGURE 2.** HSP-based massive-MIMO transmitter.

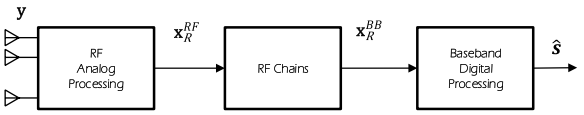


**FIGURE 3.** HSP-based massive-MIMO receiver.

The received signal can then be written as

$$\mathbf{y} = \mathbf{H}\mathbf{x} + \mathbf{n}, \tag{2}$$

where $\mathbf{H} \in \mathbb{C}^{N_R\times N_T}$ is the MIMO flat fading channel matrix such that $\mathbb{E}\{\|\mathbf{H}\|_F^2\} = N_T N_R$ and $\mathbf{n} \sim \mathcal{CN}(\mathbf{0}, \sigma^2\mathbf{I}_{N_R})$ is an additive white Gaussian noise (AWGN) vector. The decoded symbols after hybrid processing can be expressed as

$$\hat{\mathbf{s}} = \mathbf{D_D}\mathbf{D_A}\mathbf{y}, \tag{3}$$

where $\mathbf{D_D} \in \mathbb{C}^{K\times M_R}$ and $\mathbf{D_A} \in \mathbb{U}^{M_R\times N_R}$ are the digital and analog combiners, respectively.

### B. GENERALIZED HSPSYSTEM FORMULATION

In this work, we consider a more general formulation for HSP that extends the cascaded structure of analog and digital linear transformations presented in Subsection II-A. We will see that this formulation can in fact bring simplifications to the conventional linear MIMO precoding/combining techniques.

In the generalized HSP-based massive-MIMO transmitter, as shown in Fig. 2, the symbol vector $\mathbf{s}$ is first applied as input to the digital signal processor, whose output is a baseband signal vector expressed as

$$\mathbf{x}_T^{BB} = \mathscr{F}_T(\mathbf{s}) \in \mathbb{C}^{M_T}, \tag{4}$$

where $\mathscr{F}_T : \mathscr{A}^K \to \mathbb{C}^{M_T}$ is the corresponding mapping from $\mathscr{A}^K$ to $\mathbb{C}^{M_T}$. Then, $M_T$ parallel RF chains convert the

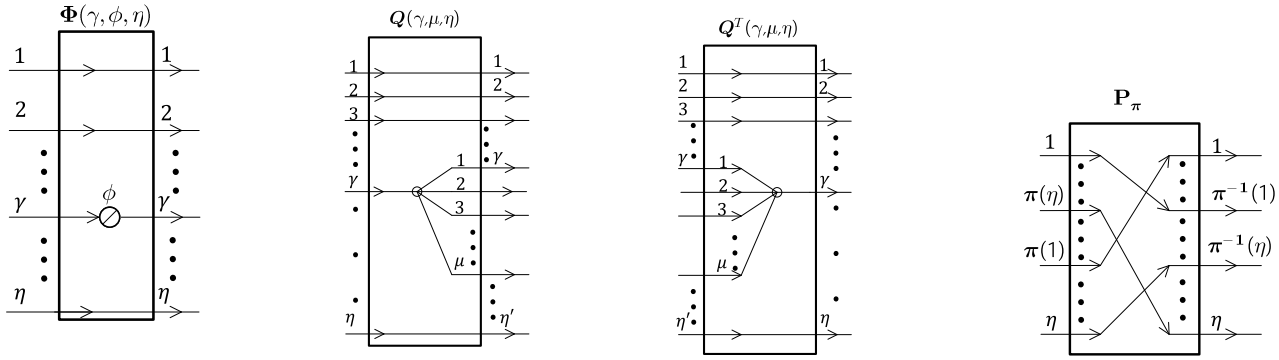


(a) Single phase-shifter. (b) Single power divider. (c) Single power combiner. (d) Permutation matrix.

**FIGURE 4.** Matrix representation of ASP components.

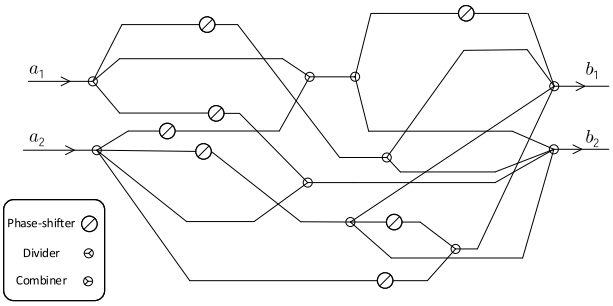


**FIGURE 5.** An example of an arbitrary ASP network.

baseband signal vector $\mathbf{x}_T^{BB}$ into a bandpass modulated RF signal vector $\mathbf{x}_T^{RF}$. The latter is next input to the ASP network whose output is the transmit signal vector, which can be expressed as

$$\mathbf{x}_T = \sqrt{\rho}\,\mathscr{G}_T(\mathbf{x}_T^{RF}) \in \mathbb{C}^{N_T}, \tag{5}$$

where $\mathscr{G}_T : \mathbb{C}^{M_T} \to \mathbb{C}^{N_T}$ is the corresponding mapping.

As shown in Fig. 3, the received RF signal $\mathbf{y}$ following from the noisy MIMO transmission as in (2) is first applied as input to the ASP network, yielding

$$\mathbf{x}_R^{RF} = \mathscr{G}_R(\mathbf{y}) \in \mathbb{C}^{M_R}, \tag{6}$$

where $\mathscr{G}_R : \mathbb{C}^{N_R} \to \mathbb{C}^{M_R}$. The RF signal vector $\mathbf{x}_R^{RF}$ is next converted to baseband vector $\mathbf{x}_R^{BB}$ by $M_R$ RF chains. Finally, $\mathbf{x}_R^{BB}$ is processed in digital domain to obtain the decoded symbols

$$\hat{\mathbf{s}} = \mathscr{F}_R(\mathbf{x}_R^{BB}). \tag{7}$$

where $\mathscr{F}_R : \mathbb{C}^{M_R} \to \mathscr{A}^K$.

While only a power constraint is imposed on the baseband mappings $\mathscr{F}_R$ and $\mathscr{F}_T$, the RF mappings $\mathscr{G}_R$ and $\mathscr{G}_T$ must be implemented by RF analog components which constrain these transformations as discussed in the following section.

## III. ANALOG SIGNAL PROCESSING NETWORK

In this section, aiming at exploiting the full potential of the analog domain, we develop a mathematical formulation for the ASP network represented by the RF mappings $\mathscr{G}_T$ and $\mathscr{G}_R$ in the previous section. Specifically, instead of focusing on the conventional analog beamformer structure used in the recent literature [13]–[21], we consider an arbitrarily connected network of phase-shifters, power dividers and power combiners. In our developments, signal-flow graph concepts are used which provide valuable insights for analysis of linear networks [30], [31].

Let us start by formally introducing the individual RF components comprising the ASP networks. The input-output (I/O) relationship of a phase-shifter is given by $b = e^{j\theta}a$ where $a, b \in \mathbb{C}$ are the input and output, respectively, and $\theta \in [0, 2\pi]$ controls the phase difference between them. In this work, in order to explore the performance limits of ASP networks and find a compact representation for any arbitrarily connected ASP with common RF components, we consider infinite resolution phase shifters.[1] The passive power combiner and power divider are implemented by the same RF multi-port network but their port configuration is different. For instance, the ideal $\mu$-way Wilkinson power divider is an $\mu+1$ port RF network which can act as an equi-power divider if the input signal is applied to its port 1 and the outputs are taken from ports 2 to $\mu+1$ [32]. Conversely, it acts as a combiner if the inputs are applied to port 2 to $\mu+1$ and the output is taken from port 1.

To obtain a unified model for any possible ASP network with $M$ input ports and $N$ output ports using primary modules (i.e., phase-shifter, power divider and power combiner), we first present a convenient multi-port matrix representation of each component. We also include a permutation operation which does not require additional hardware and is used mainly for the sake of mathematical simplification. The I/O relationship of the components are defined below in terms

[1] The proposed ASP architecture can still be applied with finite-precision phase-shifters, but some of the results derived in the paper will become approximative. This raises interesting questions from a theoretical perspective, e.g.: how to characterize the effect of phase-shifter quantization on the performance of the overall ASP network, and how to select the quantization levels of the phase-shifters to ensure a given accuracy in the final ASP design? These questions remain of interest for future research.

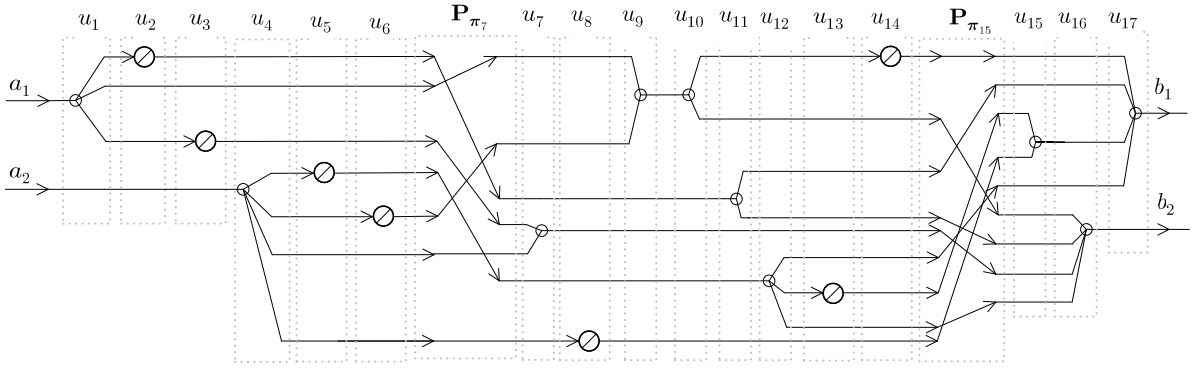


**FIGURE 6.** Applying Proposition 1 to the ASP network in Fig. 5.

of their input and outputs represented by vector $\mathbf{a}$ and $\mathbf{b}$, respectively.

- *Single phase-shifter*: As illustrated in Fig. 4, for vector $\mathbf{a}, \mathbf{b} \in \mathbb{C}^{\eta}$, the corresponding $\eta \times \eta$ matrix only changes the phase of the $\gamma^{th}$ element of the RF input signal $\mathbf{a}$, which can be expressed as

$$\mathbf{b} = \Phi(\gamma, \phi, \eta)\mathbf{a}, \tag{8a}$$
$$\Phi(\gamma, \phi, \eta) = \text{bd}(\mathbf{I}_{\gamma-1}, e^{j\phi}, \mathbf{I}_{\eta-\gamma}) \in \mathbb{C}^{\eta\times\eta}. \tag{8b}$$

- *Single power divider*: For input vector $\mathbf{a} \in \mathbb{C}^{\eta}$ and output vector $\mathbf{b} \in \mathbb{C}^{\eta'}$, the corresponding $\eta' \times \eta$ matrix divides the $\gamma^{th}$ element of the input RF signal into $\mu$ equi-power signals and the remaining RF branches are not altered, and hence, $\eta' = \eta + \mu - 1$. As illustrated in Fig. 4b, this operation can be described by a block diagonal matrix

$$\mathbf{b} = \mathbf{Q}(\gamma, \mu, \eta)\mathbf{a}, \tag{9a}$$
$$\mathbf{Q}(\gamma, \mu, \eta) = \text{bd}(\mathbf{I}_{\gamma-1}, \frac{1}{\sqrt{\mu}}\mathbf{1}_{\mu}, \mathbf{I}_{\eta-\gamma}). \tag{9b}$$

- *Single power combiner*: This transformation can be represented by the transpose of the single power divider matrix $\mathbf{Q}(\gamma, \mu, \eta)$. Consequently, for input vector $\mathbf{a} \in \mathbb{C}^{\eta'}$ and output vector $\mathbf{b} \in \mathbb{C}^{\eta}$ the corresponding matrix combines $\mu$ adjacent RF signals into the $\gamma^{th}$ output signal and the rest of the RF branches are not altered. As seen from Fig. 4c, we can write

$$\mathbf{b} = \mathbf{Q}^t(\gamma, \mu, \eta)\mathbf{a}. \tag{10}$$

- *Permutation matrix*: This transformation shown in Fig. 4d corresponds to rearrangement of the elements of vector $\mathbf{a} \in \mathbb{C}^{\eta}$ into vector $\mathbf{b} \in \mathbb{C}^{\eta}$ according to a permutation $\pi : \{1, \ldots, \mu\} \rightarrow \{1, \ldots, \mu\}$. This can be expressed as

$$\mathbf{b} = \mathbf{P}_{\pi}\mathbf{a}, \tag{11}$$

where $\mathbf{P}_{\pi} = [\mathbf{e}_{\pi_1}, \ldots, \mathbf{e}_{\pi_M}]^t$, and $\mathbf{e}_i$ denotes a column vector of zeros except for its $i^{th}$ element which is one (see ).

Having introduced a matrix representation of the RF components, we can now seek the mathematical formulation for any given ASP in terms of these matrices.

*Proposition 1:* Any given RF network, with $N$ input and $M$ output ports, implemented by arbitrary feed-forward connections of $T$ RF components (i.e., phase-shifters, power combiners and power dividers) can be modeled as follows

$$\begin{aligned}\mathbf{b} &= \mathbf{A}_{u_T}(\theta_T)\mathbf{P}_{\pi_T} \ldots \mathbf{A}_{u_2}(\theta_2)\mathbf{P}_{\pi_2}\mathbf{A}_{u_1}(\theta_1)\mathbf{P}_{\pi_1}\mathbf{a} \\ &\triangleq \prod_{i=1}^{T} \mathbf{A}_{u_i}(\theta_i)\mathbf{P}_{\pi_i}\mathbf{a},\end{aligned}$$
$$\mathbf{A}_{u_i}(\theta_i) = \begin{cases} \Phi(\gamma, \phi, \eta), & \text{where } \theta_i \equiv (\gamma, \phi, \eta) \quad \text{if } u_i = 1 \\ \mathbf{Q}(\gamma, \mu, \eta), & \text{where } \theta_i \equiv (\gamma, \mu, \eta) \quad \text{if } u_i = 2 \\ \mathbf{Q}^t(\gamma, \mu, \eta), & \text{where } \theta_i \equiv (\gamma, \mu, \eta) \quad \text{if } u_i = 3, \end{cases} \tag{12}$$

where $\mathbf{a} \in \mathbb{C}^N$ and $\mathbf{b} \in \mathbb{C}^M$ are the input and output RF signals, respectively, and $\theta_i$ is a 3-tuple containing the parameters of the $i^{th}$ RF component.

*Proof:* See Appendix A. ■

To illustrate the application of this result, consider the ASP network example in Fig. 5. By using the indexing scheme introduced in the Proof of Proposition 1, this network can be reorganized as a product of basic RF transformations as shown in Fig. 6. Note that in the latter figure, permutation matrices only appear before the $7^{th}$ and $15^{th}$ RF components; for the remaining components the permutation is an identity matrix (not shown for simplicity). It is worth mentioning that the indexing is not unique and parallel components can be swapped, for instance, the order of $u_2$, $u_3$ and $u_4$ does not affect the I/O relationship of the ASP network.

In the following theorem, we present five commutative properties of matrices $\Phi(\gamma, \phi, \eta)$, $\mathbf{P}_{\pi}$, $\mathbf{Q}(\gamma, \mu, \eta)$, and $\mathbf{Q}^t(\gamma, \mu, \eta)$ which later will be used to rearrange the RF components for further simplifications.

*Theorem 1:* For each one of the following products of two basic RF component matrices on the left, there exists an equivalent matrix factorization as given on the right of the

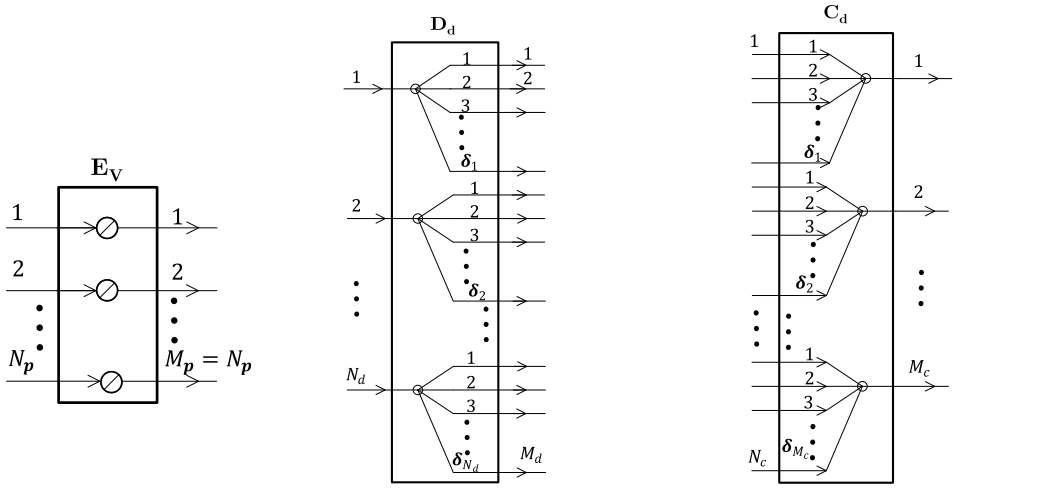


(a) Phase-shifter network. (b) Power divider network. (c) Power combiner network.

**FIGURE 7.** ASP sub-networks.

equality sign:

$$\mathbf{Q}(\gamma,\mu,\eta)\mathbf{P}_\pi = \mathbf{P}_{\pi'}\mathbf{Q}(\pi(\gamma),\mu,\eta), \quad (13)$$

$$\mathbf{P}_\pi\mathbf{Q}^t(\gamma,\mu,\eta) = \mathbf{Q}^t(\pi(\gamma),\mu,\eta)\mathbf{P}_{\pi'}, \quad (14)$$

$$\mathbf{Q}(\gamma_1,\mu_1,\eta_1)\mathbf{Q}^t(\gamma_2,\mu_2,\eta_2) = \prod_{j=1}^{J'}\mathbf{Q}^t(\gamma_j',\mu_j',\eta_j')\mathbf{P}_{\pi'} \times \prod_{j'=1}^{J''}\mathbf{Q}(\gamma_{j'}'',\mu_{j'}'',\eta_{j'}''), \quad (15)$$

$$\mathbf{Q}(\gamma_1,\mu,\eta_1)\Phi(\gamma_2,\phi,\eta_2) = \prod_{j=1}^{J}\Phi(\gamma_j',\phi_j',\eta_j') \times \mathbf{Q}(\gamma',\mu',\eta'), \quad (16)$$

$$\Phi(\gamma_1,\phi,\eta_1)\mathbf{Q}^t(\gamma_2,\mu,\eta_2) = \mathbf{Q}^t(\gamma',\mu',\eta') \times \prod_{j=1}^{J}\Phi(\gamma_j',\phi_j',\eta_j'). \quad (17)$$

The definitions of the parameters appearing on the right hand side of these identities are given in the proof.

*Proof:* See Appendix B. ■

Next, we introduce three ASP sub-networks and their compact equivalent representations; these will play a key role in establishing our main results in Theorems 2 and 3.

- *Phase-shifter network*: This sub-network is obtained by cascading $J$ basic phase shifter matrices (with accompanying permutations) of common size $N_{\mathbf{p}}$, i.e.

$$\prod_{j=1}^{J}\Phi(\gamma_j,\phi_j,N_{\mathbf{p}})\mathbf{P}_{\pi_j} = \mathbf{E}_{\mathbf{v}}\mathbf{P}_\pi, \quad (18)$$

where, as illustrated in Fig. 7

$$\mathbf{E}_{\mathbf{v}} = \mathrm{diag}(\mathbf{v}), \quad (19)$$

with $\mathbf{v} = [e^{j\phi_1}, e^{j\phi_2}, \ldots, e^{j\phi_{N_{\mathbf{p}}}}]^t \in \mathbb{U}^{N_{\mathbf{p}}}$.

- *Power divider network*: By cascading $J$ power divider matrices of compatible sizes, we obtain

$$\prod_{j=1}^{J}\mathbf{Q}(\gamma_j,\mu_j,\eta_j) = \mathbf{P}_\pi\mathbf{D_d}\mathbf{P}_{\pi'} \quad (20)$$

where, as illustrated in Fig. 7b,

$$\mathbf{D_d} = \mathrm{bd}\left(\frac{1}{\sqrt{\delta_1}}\mathbf{1}_{\delta_1}, \frac{1}{\sqrt{\delta_2}}\mathbf{1}_{\delta_2}, \ldots, \frac{1}{\sqrt{\delta_{N_d}}}\mathbf{1}_{\delta_{N_d}}, \mathbf{I}\right), \quad (21)$$

with $\mathbf{d} = [\delta_1, \delta_2, \ldots, \delta_{N_d}]^t$, and $\sum_{i=1}^{N_d}\delta_i = M_d$, which is equivalent to an RF network that divides $N_d$ RF signals into a total of $M_d$ signals. The presence of the identity matrix in (21) accounts for branches that are not divided.

- *Power combiner network*: By cascading $J$ power combiner matrices, we obtain,

$$\prod_{j=1}^{J}\mathbf{Q}^t(\gamma_j,\mu_j,\eta_j)\mathbf{P}_{\pi_j} = \mathbf{P}_\pi\mathbf{C_d}\mathbf{P}_{\pi'} \quad (22)$$

where, as illustrated in Fig. 7c,

$$\mathbf{C_d} = \mathrm{bd}\left(\frac{1}{\sqrt{\delta_1}}\mathbf{1}_{\delta_1}^t, \frac{1}{\sqrt{\delta_2}}\mathbf{1}_{\delta_2}^t, \ldots, \frac{1}{\sqrt{\delta_{M_c}}}\mathbf{1}_{\delta_{M_c}}^t, \mathbf{I}\right), \quad (23)$$

with $\mathbf{d} = [\delta_1, \delta_2, \ldots, \delta_{M_c}]$ and $\sum_{i=1}^{M_c}\delta_i = N_c$, which is equivalent to an RF network that combines $N_c$ RF signals into $M_c$ signals.

The validity of the identities in (18), (20) and (22) is demonstrated in Appendix C. We can now derive a mathematical expression for the representation of any given ASP network.

*Theorem 2:* Any arbitrarily connected feed-forward ASP network with $M$ inputs and $N$ outputs, implemented by a total number of $T$ phase-shifters, power dividers, and power

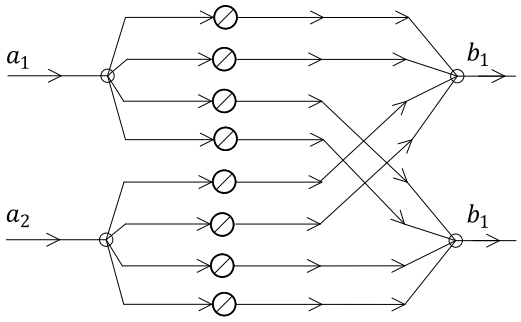


**FIGURE 8.** ASP network equivalent to the ones in Figs. 5 and 6.

combiners can be modeled as

$$\mathbf{b} = \frac{1}{\sqrt{MN}}\mathbf{A}\mathbf{a}, \tag{24a}$$

$$\mathbf{A} \in \breve{\mathbb{U}}^{N\times M}, \tag{24b}$$

where $\mathbf{a} \in \mathbb{C}^M$ and $\mathbf{b} \in \mathbb{C}^N$ are the input and output signals, respectively, and $\breve{\mathbb{U}} = \{z \in \mathbb{C}\colon |z| \leq 1\}$. That is, all the entries of matrix $\mathbf{A}$ have magnitude less or equal to 1.

*Proof:* See Appendix D ∎

Going back to our previous example in Fig. 5 and Fig. 6, the ASP network in the latter figure can be transformed into that of Fig. 8, for which the $2 \times 2$ transformation matrix $\mathbf{A}$ satisfies the condition of the theorem. Now, we investigate whether any matrix in the convex set $\breve{\mathbb{U}}^{N\times M}$ can be realized by an ASP.

*Theorem 3:* Any given matrix $\mathbf{A} \in \breve{\mathbb{U}}^{N\times M}$ can be realized by an ASP network with a total number of $T = 2MN + M + N$ RF components, i.e., $N$ dividers, $M$ combiners, and $2NM$ (unit-modulus) phase shifters, as shown in Fig. 9.

*Proof:* The output of the ASP in Fig. 9, corresponding to the input vector $\mathbf{a}$, can be expressed as

$$b_i = \frac{1}{\sqrt{2M}}\sum_{k=1}^{M}\Big(\frac{a_k}{\sqrt{2N}}e^{j\phi^1_{k,i}} + \frac{a_k}{\sqrt{2N}}e^{j\phi^2_{k,i}}\Big) \tag{25a}$$

$$= \frac{1}{\sqrt{MN}}\sum_{k=1}^{M}a_k\Big(\frac{1}{2}\sum_{l=1}^{2}e^{j\phi^l_{k,i}}\Big). \tag{25b}$$

In (25a), since $b_i$ is the output of a $2M$-way combiner, the normalization factor $\frac{1}{\sqrt{2M}}$ appears from (9). Similarly, the $k^{th}$ input, i.e., $a_k$ is divided into $2N$ branches which according to (9) introduces a normalization factor of $\frac{1}{\sqrt{2N}}$. Subsequently, for a given $\mathbf{A} \in \breve{\mathbb{U}}^{N\times M}$, we have $A_{ki} \leq 1$, and by invoking Lemma 2, there exist angles $\phi^l_{k,i}$'s such $A_{ki} = \frac{1}{L}\sum_{l=1}^{L}e^{j\phi^l_{k,i}}$ where the minimum possible value of $L$ is two, i.e., $A_{ki} = \frac{1}{2}(e^{j\phi^1_{k,i}} + e^{j\phi^2_{k,i}})$. Therefore, we have:

$$b_i = \frac{1}{\sqrt{MN}}\sum_{k=1}^{M}A_{ki}a_k, \tag{26}$$

where $\mathbf{A} \in \breve{\mathbb{U}}^{N\times M}$. Moreover, $2M$ phase-shifters are required for each element of $\mathbf{b}$ and consequently, a minimum of $2MN$ phase-shifters are needed. ∎

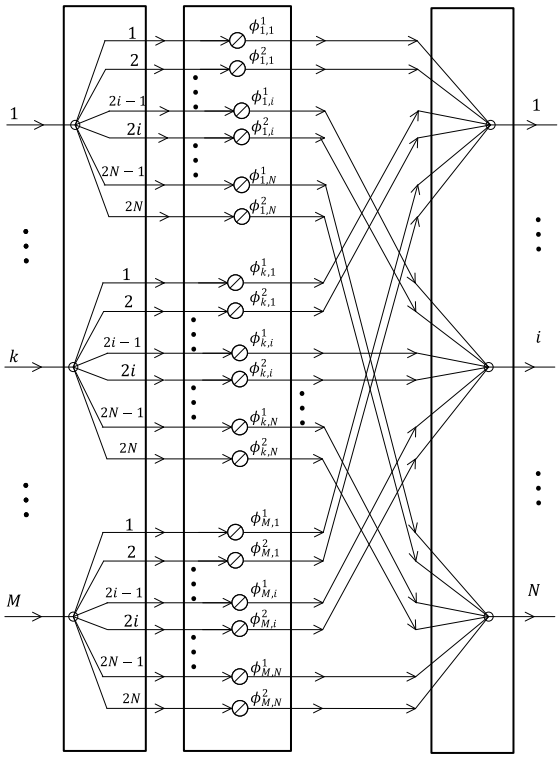


**FIGURE 9.** Proposed ASP architecture.

*Remark 1:* The significant result of Theorem 3, is that any $\mathbf{A} \in \breve{\mathbb{U}}^{N\times M}$ can be implemented with an ASP structure using conventional RF components, i.e. combiners, dividers and phase shifters, whose input-output relationship is not bound to the unit modulus constraint. That is, while the individual phase-shifter components satisfy this constraint, the overall transformation matrix implemented by the proposed structure in Fig. 9 is no longer restricted to the unit modulus constraint. Thus, the troubling non-convexity constraint found in the literature on hybrid beamforming literature can be lifted from the design optimization problems.

*Remark 2:* According to the above proof, non-unique solutions for phase-shifter may exist. This additional degree of freedom can be considered when designing the ASP network based on the requirements and constraints of the analog system. By writing $A_{p,q} = |A_{p,q}|\exp(j\angle Ap, q)$, one possible solution for $\phi^1_{k,i}$ and $\phi^2_{k,i}$ is given by

$$\phi^1_{k,i} = \angle Ap, q + \cos^{-1}(|Ap, q|) \tag{27a}$$

$$\phi^2_{k,i} = \angle Ap, q - \cos^{-1}(|Ap, q|). \tag{27b}$$

It is worth noting that in the conventional hybrid structure $T = MN + M + N$ RF components are required [13]–[21]. In contrast, the proposed ASP structure requires MN additional phase-shifters, for a total of $T = 2MN + M + N$ RF components. These additional components, when employed as in Fig. 9, allow to lift the constant modulus constraint for the overall transformation.

*Remark 3:* It is worth mentioning that since for wide-band systems it is desirable to have a common ASP network for the entire band [25]–[27] the proposed structure can be used for MIMO-OFDM systems. Particularly, since the proposed ASP structure is not bound to constant modulus constraint, it simplifies the design of hybrid MIMO-OFDM beamformers.

## IV. TRANSMITTER AND RECEIVER DESIGN WITH GENERALIZED HSP

While the previous section focused on the realization of the RF mappings $\mathscr{G}_R$ and $\mathscr{G}_T$, as defined in (5) and (6), using basic RF components, in this section we turn our attention to the baseband mappings $\mathscr{F}_R$ and $\mathscr{F}_T$ as defined in (7) and (4), respectively. To this end, we consider the ASP network in Fig. 9 for $\mathscr{G}_T$ and $\mathscr{G}_R$ and consequently, (5) and (6) are replaced by:

$$\mathscr{G}_T(\mathbf{x}_T^{RF}) = \mathbf{A}_T\mathbf{x}_T^{RF}, \tag{28a}$$

$$\mathscr{G}_R(\mathbf{y}) = \mathbf{A}_R\mathbf{y}, \tag{28b}$$

where $\mathbf{A}_T \in \breve{\mathbb{U}}^{N_T\times M_T}$ and $\mathbf{A}_R \in \breve{\mathbb{U}}^{M_R\times N_R}$. We first focus on the transmitter and then on the receiver design.

### A. HSPDESIGN AT THE TRANSMITTER

Considering (4), (5), and (28a), the transmitted signal of the generalized HSP can be written as follows:

$$\mathbf{x}_T = \sqrt{\rho}\mathbf{A}_T\mathscr{F}_T(\mathbf{s}). \tag{29}$$

In the literature on hybrid beamforming, $\mathscr{F}_T$ is usually a linear transformation, i.e., $\mathbf{x}_T = \sqrt{\rho}\mathbf{A}_T\mathbf{P}\mathbf{s}$, where $\mathbf{P} \in \mathbb{C}^{M_T\times K}$ is the precoding matrix. We first explore the properties and implementation of $\mathscr{F}_T$, and then discuss the design of $\mathscr{F}_T$ and $\mathbf{A}_T$ at the HSP-based transmitter.

Let $\mathscr{D}_T(\mathbf{s})$ denote the transformation that generates the desired transmitted signal from the given vector symbol $\mathbf{s}$. In effect, this function can represent a generic communication techniques at the transmitter side. For instance, the optimal eigen-mode precoding is obtained by solving the following problem:

$$\max_{\mathbf{P}} \ \log_2\det(\mathbf{I}_{N_R} + \mathbf{H}\mathbf{P}\mathbf{P}^H\mathbf{H}^H), \tag{30a}$$

$$\text{s.t. } \mathrm{Tr}(\mathbf{P}\mathbf{P}^H) \le P_T. \tag{30b}$$

The solution is given by

$$\mathbf{P} = \mathbf{V}\Upsilon, \tag{31}$$

where the diagonal weight matrix $\Upsilon$ is calculated via water filling [33] and $\mathbf{V}$ is a unitary matrix obtained from singular value decomposition of the channel matrix, i.e.,

$$\mathbf{H} = \mathbf{U}\Sigma\mathbf{V}^H. \tag{32}$$

Consequently, for this particular precoding scheme we have

$$\mathscr{D}_T(\mathbf{s}) = \mathbf{V}\Upsilon\mathbf{s}. \tag{33}$$

Note that nonlinear beaforming, channel estimation, space-time coding and many other techniques can also be represented by $\mathscr{D}_T(\mathbf{s})$.

From (29), in order to generate the same transmit signal as a given $\mathscr{D}_T(\mathbf{s})$ via an HSP-based transmitter, we need to find $\mathbf{A}_T$ and $\mathscr{F}_T(.)$ such that

$$\mathbf{A}_T\mathscr{F}_T(\mathbf{s}) = \mathscr{D}_T(\mathbf{s}), \tag{34}$$

holds for all symbol vectors $\mathbf{s}$. Hence, since $\mathscr{D}_T(\mathbf{s})$ is given, $\mathscr{F}_T(\mathbf{s})$ can be defined as the following set set, or multi-valued function:

$$\mathscr{F}_T(\mathbf{s}) \triangleq \{\mathbf{x} \in \mathbb{C}^K : \mathbf{A}_T\mathbf{x} = \mathscr{D}_T(\mathbf{s})\}. \tag{35}$$

Note that while it might be very difficult to explicitly construct the mapping $\mathscr{F}_T(.)$, obtaining its output, i.e., $\mathscr{F}_T(\mathbf{s})$ is simple because the value of $\mathscr{D}_T(\mathbf{s})$ is available. In other words, since the output of the HSP-based transmitter is given, i.e. $\mathscr{D}_T(\mathbf{s})$, it is sufficient to calculate the desired output of $\mathscr{F}_T(.)$ rather than implementing the mapping itself.

From (4) and (35), we can rewrite (34) as

$$\mathbf{A}_T\mathbf{x}_T^{BB} = \mathscr{D}_T(\mathbf{s}) \tag{36}$$

which means that in general the HSP objective is *to find* $\mathbf{A}_T$ *and* $\mathbf{x}_T^{BB}$ *such that* (36) *is satisfied for the given* $\mathscr{D}_T(\mathbf{s})$. This objective guarantees that the HSP-based system achieves the same performance as the FD one, i.e., $\mathscr{D}_T(\mathbf{s})$. However, many variations can be derived according to the conditions and constraints of the system, which opens new avenues for investigation in this area.

In practice, depending on the system constraints, one may wish to design $\mathbf{A}_T$, $\mathbf{x}_T^{BB}$ and possibly some other system parameters represented by vector $\mathbf{p}$ on the basis of some optimization criterion. For instance, the following generic optimization problem can be used for obtaining the HSP parameters,

$$\min_{\mathbf{A}_T,\mathbf{x}_T^{BB},\mathbf{p}} \ \mathbb{E}\{\|\mathbf{A}_T\mathbf{x}_T^{BB} - \mathscr{D}_T(\mathbf{s})\|^2\}, \tag{37a}$$

$$\text{s.t. } C(\mathbf{A}_T, \mathbf{x}_T^{BB}, \mathbf{p}), \tag{37b}$$

where $C(\mathbf{A}_T, \mathbf{x}_T^{BB}, \mathbf{p})$ represents the system constraints. Alternatively, this could be formulated as

$$\underset{\mathbf{A}_T,\mathbf{x}_T^{BB},\mathbf{p}}{\text{optimize}} f(\mathbf{A}_T, \mathbf{x}_T^{BB}, \mathbf{p}), \tag{38a}$$

$$\text{s.t. } \mathbf{A}_T\mathbf{x}_T^{BB} = \mathscr{D}_T(\mathbf{s}). \tag{38b}$$

where $f(.)$ is the chosen cost function based on the objectives of the system. Note that the power constraint is not necessary as it can be taken into account when designing $\mathscr{D}_T(\mathbf{s})$. One obvious choice is $f(\mathbf{A}_T, \mathbf{x}_T^{BB}, \mathbf{p}) = 1$, in which case $\mathbf{A}_T$ must be designed such that for some set $\mathbb{S} \subset \mathscr{A}^K$, we have $\mathscr{D}_T(\mathbf{s}) \in \mathrm{span}(\mathbf{A}_T)$, $\forall\mathbf{s} \in \mathbb{S}$, where $\mathrm{span}(\mathbf{A}_T)$ denotes the span of $\mathbf{A}_T$. Consequently, the baseband signal is obtained from $\mathbf{x}_T^{BB} = \mathbf{A}_T^{\dagger}\mathscr{D}_T(\mathbf{s})$ where $\mathbf{A}_T^{\dagger}$ is the Moore Penrose inverse of matrix $\mathbf{A}_T$. In what follows, we present different cost functions for designing precoding matrices with HSP.

#### 1) UNCONSTRAINED FD PRECODING FOR $M_T \geq K$

For $M_T \geq K$ it is possible to realize any given FD precoder. As an example, we explore optimal eigen-mode precoding, although any other precoding matrix can be obtained in the same fashion. We first consider the case $M_T = K$ and subsequently discuss the modifications needed for $M_T \geq K$.

From (33) and (36), both $\mathbf{A}_T$ and $\mathbf{x}_T^{BB}$ must be designed such that

$$\mathbf{A}_T \mathbf{x}_T^{BB} = \mathbf{V}\Upsilon\mathbf{s}. \tag{39}$$

Since $\mathbf{A}_T$ is of size $N_T \times M_T$, this problem for $M_T = K$ has the following simple solution

$$\mathbf{A}_T = \frac{1}{p_0}\mathbf{V}\Upsilon, \tag{40a}$$

$$\mathbf{x}_T^{BB} = p_0\mathbf{s}, \tag{40b}$$

where $p_0 = \|\text{vec}(\mathbf{V}\Upsilon)\|_\infty$.

In the case $M_T > K$, one possible solution that achieves the same performance as the FD precoding is to append $M_T - K$ zeros to the solution $\mathbf{x}_T^{BB}$ in (40b) and set the corresponding columns of $\mathbf{A}_T$ in (40a) to zero.

Note that no constraint is enforced on the system and similar to existing hybrid solutions in the literature, $\mathbf{A}_T$ must be updated according to the channel coherence time, denoted as $T_c$ in the sequel. Since $\mathbf{s}$ changes after every symbol duration $T_s$, $\mathbf{x}_T^{BB}$ is also updated every $T_s$.

#### 2) UNCONSTRAINED FD PRECODING FOR $M_T < K$

In this case, from using either (38) or (38), it is possible to obtain various hybrid beamformer designs depending on the system requirements. Here, we aim at minimizing the Euclidean distance between the eigen-mode FD precoder in (31) and the hybrid beamforming matrix $\mathbf{A}_T$. However, since the former has size $N_T \times M_T$ while the latter has size $N_T \times K$, we first find a beamforming matrix $\hat{\mathbf{A}}_T$ of size $N_T \times M_T$ subject to a rank $M_T$ constraint, i.e.,

$$\min_{\hat{\mathbf{A}}_T} \ \|\hat{\mathbf{A}}_T - \mathbf{V}\Upsilon\|^2 \tag{41a}$$

$$\text{s.t. } \text{rank}(\hat{\mathbf{A}}_T) = M_T. \tag{41b}$$

Since here $\Upsilon = [\text{diag}(\upsilon_1, \upsilon_2, \ldots, \upsilon_K), \mathbf{0}_{K\times(N_T-K)}]^t$, we can write the solution for the above problem as

$$\hat{\mathbf{A}}_T = \mathbf{V}\begin{bmatrix}\text{diag}(\upsilon_1, \upsilon_2, \ldots, \upsilon_{M_T}, 0, \ldots, 0)\\ \mathbf{0}_{(N_T-K)\times K}\end{bmatrix}. \tag{42}$$

Now by defining

$$\mathbf{A}_T = \mathbf{V}\begin{bmatrix}\text{diag}(\upsilon_1, \upsilon_2, \ldots, \upsilon_{M_T})\\ \mathbf{0}_{(N_T-M_T)\times M_T}\end{bmatrix}, \tag{43}$$

we can obtain $\mathbf{x}_T^{BB}$ by solving

$$\min_{\mathbf{x}_T^{BB}} \ \|\mathbf{A}_T\mathbf{x}_T^{BB} - \mathbf{V}\Upsilon\mathbf{s}\|^2, \tag{44}$$

which yields

$$\mathbf{x}_T^{BB} = [\mathbf{I}_{M_T}, \mathbf{0}_{M_T\times(K-M_T)}]\mathbf{s}. \tag{45}$$

#### 3) MINIMUM NUMBER OF RF CHAINS WITH FAST PHASE-SHIFTERS

If we do not have a constraint on the update rate of the analog components, we can reduce the number of RF chains by solving the following problem

$$\min_{\mathbf{A}_T, \mathbf{x}_T^{BB}} \ M_T, \tag{46a}$$

$$\text{s.t. } \mathbf{A}_T\mathbf{x}_T^{BB} = \mathscr{D}_T(\mathbf{s}). \tag{46b}$$

This problem is shown to have non-unique solution for $M_T = 1$ where $\mathscr{D}_T(\mathbf{s}) = \mathbf{V}\Upsilon\mathbf{s}$ in [23] but essentially the same solution is valid for any other transmit function $\mathscr{D}_T(\mathbf{s})$. Note that in this case the ASP must be updated after every symbol duration $T_s$.

### B. HSPDESIGN AT THE RECEIVER

Similar to the previous subsection, let us assume that the ideal FD decoder that maps the received RF signal $\mathbf{y}$ into the detected symbols $\hat{\mathbf{s}}$, represented by the mapping $\mathscr{D}_R(\mathbf{y})$, is known. Since in massive-MIMO systems beamforming and multiplexing are key techniques, linear detection is of great interest due to its simplicity. In this case, which is considered in our discussion, $\mathscr{D}_R(\mathbf{y}) = \mathbf{Z}\mathbf{y}$ where $\mathbf{Z} \in \mathbb{C}^{K\times N_R}$ is the FD combiner matrix. However, at the price of increased computational complexity, $\mathscr{D}_R(\mathbf{y})$ can be extended to more sophisticated detectors such as maximum likelihood or sphere decoding.

By substituting (6) and (28b) in (7), the estimated signal at the receiver is written as:

$$\hat{\mathbf{s}} = \mathscr{F}_R\big(\mathbf{A}_R(\mathbf{H}\mathbf{x}_T + \mathbf{n})\big). \tag{47}$$

Clearly, the same approach used in Subsection IV-A for realizing the transformation $\mathscr{F}_T(.)$ cannot be applied here because the desired output of $\mathscr{F}_R(.)$ is unknown, i.e., we need this mapping to implement the decoding function. Ideally, we want to find a mapping $\mathscr{F}_R(\cdot)$ and $\mathbf{A}_R$ such that

$$\mathscr{F}_R\big(\mathbf{A}_R\mathbf{y}\big) = \mathscr{D}_R(\mathbf{y}), \tag{48}$$

or all $\mathbf{y}$. Similar to the HSP literature [13]–[21], we consider linear transformation for the baseband processing, i.e., $\mathscr{F}_R(\mathbf{x}_R^{BB}) = \mathbf{W}\mathbf{x}_R^{BB}$ where $\mathbf{W} \in \mathbb{C}^{K\times M_R}$ is the corresponding transformation matrix; however, extension to types of transformations is straightforward by using (48). Consequently, the following generic optimization problem can be considered for obtaining the HSP parameters:

$$\min_{\mathbf{A}_R, \mathbf{W}, \mathbf{p}} \ \mathbb{E}\{\|\mathbf{W}\mathbf{A}_R - \mathbf{Z}\|_F^2\}, \tag{49a}$$

$$\text{s.t. } C(\mathbf{A}_R, \mathbf{W}, \mathbf{p}), \tag{49b}$$

where $C(\mathbf{A}_R, \mathbf{W}, \mathbf{p})$ represents the system constraints. Alternatively, this could be formulated as

$$\underset{\mathbf{A}_R, \mathbf{W}, \mathbf{p}}{\text{optimize}} f(\mathbf{A}_R, \mathbf{W}, \mathbf{p}), \tag{50a}$$

$$\text{s.t. } \mathbf{W}\mathbf{A}_R = \mathbf{Z}, \tag{50b}$$

where $f(.)$ is a cost function designed to satisfy the requirements of the system. In what follows, FD combining for point-to-point MIMO is presented as an example.

#### 1) UNCONSTRAINED FD COMBINING FOR $M_R \geq K$

We first consider the case where $M_R = K$ and subsequently discuss the case $M_R > K$. The optimal FD combiner for a point-to-point MIMO can be obtained from

$$\max_{\mathbf{Z}} \ \log_2 \det\left(\mathbf{I}_K + \rho(\mathbf{Z}\mathbf{Z}^H)^{-1}\mathbf{Z}\mathbf{H}\mathbf{H}^H\mathbf{Z}^H\right). \tag{51}$$

From (32), the solution is given by

$$\mathbf{Z}^H = \mathbf{U}^a. \tag{52}$$

where $\mathbf{U} = [\mathbf{U}^a, \mathbf{U}^b]$ and $\mathbf{U}^a$ contains the first $K$ columns of $\mathbf{U}$, corresponding to the $K$ dominant singular values of the channel matrix $\mathbf{H}$. Thus, $\mathbf{A}_R$ and $\mathbf{W}$ must be jointly designed such that

$$\mathbf{W}\mathbf{A}_R = \mathbf{Z}, \tag{53}$$

where $\mathbf{A}_R \in \breve{\mathbb{U}}^{M_R \times N_R}$. Note that if $M_T = K$, for any FD combiner $\mathbf{Z} \in \mathbb{C}^{K \times N_R}$, this problem has the following solution

$$\mathbf{A}_R = \frac{1}{p_1}\mathbf{Z}, \tag{54a}$$

$$\mathbf{W} = p_1\mathbf{I}_K, \tag{54b}$$

where $p_1 = \|\mathrm{vec}(\mathbf{Z})\|_\infty$.

The above design can be extended to the case $M_R > K$, although here including more RF chains adds to the cost and complexity of the system while no improvement is gained. One trivial solution that guarantees the same performance as the FD solution is to set the additional $M_R - K$ columns of $\mathbf{W}$ to 0, i.e., using $\mathbf{W} = p_1[\mathbf{I}_K, \mathbf{0}_{K\times(M_R-K)}]$.

The FD realization for the multi-user case can be similarly obtained. First (51) must be replaced by the desired optimization problem for finding the FD combiner. Analog and digital combiners are then calculated by (54).

#### 2) FD COMBINING FOR $M_T < K$

In the case of linear decoding, there must be at least $K$ independent equations to recover $K$ transmitted symbols. Hence, the minimum number of required RF chains is $M_R = K$. Consequently, combiner design for $M_R < K$ is not practical in this case.

#### 3) MINIMUM NUMBER OF RF CHAINS WITH FAST PHASE-SHIFTERS

Even with the same assumption as in Subsection IV-A.3, i.e. the phase-shifters can be updated every $T_s$, at least $K$ RF chains are required. Since only the channel matrix is known at the receiver which changes each $T_c$, a faster update rate of the phase-shifters does not provide any extra degrees of freedom and hence does not help in reducing the number of RF chains at the receiver. Consequently, the minimum number of possible RF chains for digital linear combining is $M = K$.

## V. SIMULATION RESULTS

In this section, we present simulation results for different scenarios and compare the FD system with our proposed hybrid architecture as well as existing hybrid designs in the literature.

The following channel models is used for all the simulations,

$$\mathbf{H} = \sqrt{\frac{N_T N_R}{N_c N_{\text{ray}}}} \sum_{i=1}^{N_c}\sum_{j=1}^{N_{\text{ray}}} \alpha_{ij}\mathbf{a}_r(\theta_{ij}^r)\mathbf{a}_t(\theta_{ij}^t)^H, \tag{55}$$

where $N_c = 5$ is the number of clusters, and $N_{\text{ray}} = 10$ is the number of rays in each cluster. Similar to [14], [27], the path gains are independently generated as $\alpha_{ij} \sim \mathcal{CN}(0, 1)$. The transmit and receive antenna responses are denoted by $\mathbf{a}_r(\theta_{ij}^r)$ and $\mathbf{a}_t(\theta_{ij}^t)$ respectively, where

$$\mathbf{a}(\phi) = \frac{1}{\sqrt{N}}[1, e^{j\pi\sin(\phi)}, \ldots, e^{j(N-1)\pi\sin(\phi)}], \tag{56}$$

for uniform linear arrays of size $N$. The angles of arrival $\theta_{ij}^r$ and departure $\theta_{ij}^t$ are independently generated according to the Laplacian distribution with the mean cluster angles $\bar{\theta}_{ij}^r$ and $\bar{\theta}_{ij}^t$, uniformly distributed in $[0, 2\pi]$. The angular spread is 10 degrees within each cluster. We further assume that the channel estimation and system synchronization are perfect.

For the massive MIMO simulations, the number of antennas $N_T$ and $N_R$ vary between 2 and 64; larger values are used for UM-MIMO, larger number of antennas are used, as later indicated. For the proposed and existing hybrid designs, the number of RF chains and transmitted symbols are set as $M_T = M_R = K$. Unless otherwise indicated, we set $K = 2$ and 64-QAM modulation is used for all the simulations. For the FD systems, we set $M_T = N_T$ and $M_R = N_R$, while the same value as for the hybrid designs is used.

Simulation results are presented for the optimal FD precoder and combiner, our proposed hybrid precoder and combiner realization of FD in Subsections IV-A.1 and IV-B.1, as well as selected hybrid designs from [14], [27]. For $M$ RF chains and $N$ antennas, the proposed and the conventional structures require $T = 2MN + M + N$ and $T = MN + M + N$ RF components, respectively.

### A. BIT ERROR RATE (BER) PERFORMANCE

BER performance versus SNR (SNR$= \rho/\sigma^2$) for three different setups is shown in Fig. 10 to 12. Fig. 10 presents the results for a massive-MIMO system with $N_T = N_R = 64$ antennas (and $M_T = M_R = 2$ RF chains). The downlink BER performance of a massive-MIMO BS with $N_T = 64$ antennas transmitting to a single user with $N_R = 2$ antenna is shown in Fig. 11, while the uplink BER performance for the system is shown in Fig. 12. It can be seen that in all the simulated scenarios the proposed hybrid realization matches the performance of the FD systems while outperforming the existing hybrid designs. The FD systems require $M_T = M_R = 64$ RF chains whereas the proposed design achieves the same performance with only 2 RF chains. Consequently, the proposed

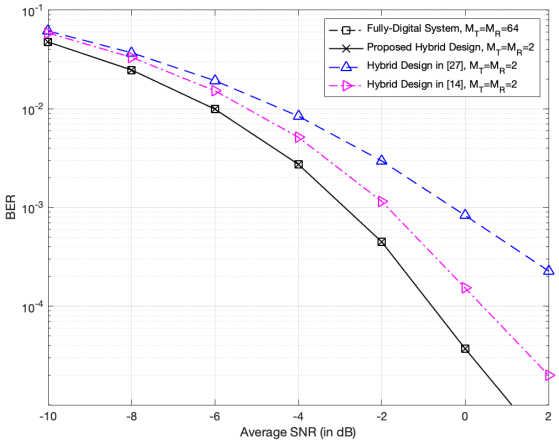


**FIGURE 10.** BER versus SNR of different methods for a point-to-point massive-MIMO system with $N_T = N_R = 64$.

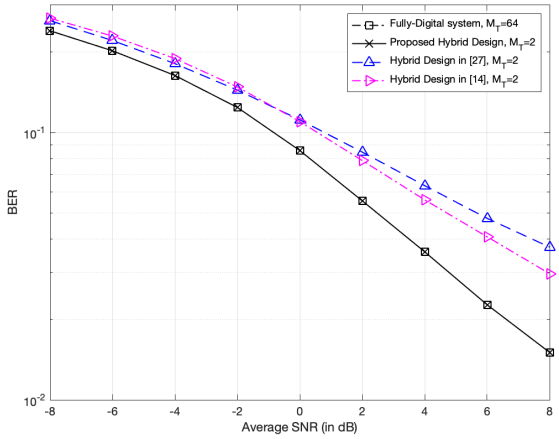


**FIGURE 11.** BER versus SNR of different methods for a downlink connection with $N_T = 64$ antenna massive-MIMO BS and a single user with $N_R = 2$ antennas.

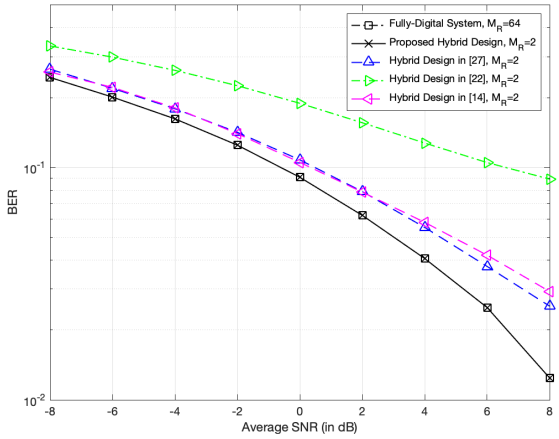


**FIGURE 12.** BER versus SNR of different methods for an uplink connection with $N_R = 64$ antenna massive-MIMO BS and a single user with $N_T = 2$.

design outperforms the existing hybrid designs with the same number of RF chains. As discussed in Subsections IV-A.1 and IV-B.1, the proposed hybrid design generates the same

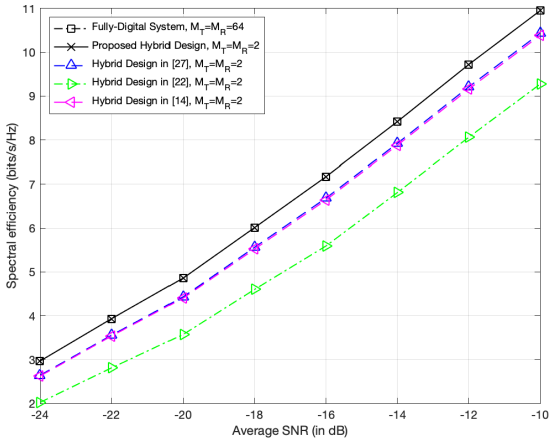


**FIGURE 13.** Spectral efficiency versus SNR of different methods for a point-to-point massive-MIMO system with $N_T = N_R = 64$.

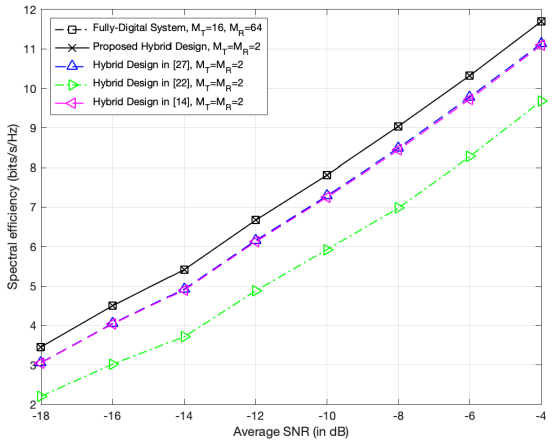


**FIGURE 14.** Spectral efficiency versus SNR of different methods for an uplink connection with $N_R = 64$ antenna massive-MIMO BS and a single user with $N_T = 16$ antennas.

signals as the FD system with limited number of RF chains by employing the proposed ASP network. In particular, since the RF output of the proposed structure is identical to that of the desired FD system, the same performance as the optimal FD beamforming can be achieved.

### B. SPECTRAL EFFICIENCY

The spectral efficiency (in bits/s/Hz) of optimal FD beamforming, proposed hybrid realizations of FD as well as the hybrid designs from [14], [22], [27] for massive-MIMO system with $N_T = N_R = 64$ antennas is shown in Fig. 13. The spectral efficiency of an uplink connection for a single user with $N_T = 16$ antennas and a massive-MIMO BS with $N_R = 64$ antennas is presented in Fig. 14. Furthermore, Fig. 15 shows the spectral efficiency of a downlink connection for a massive-MIMO BS with $N_T = 64$ antennas and a single user with $N_R = 4$ antennas. As expected, the proposed ASP-based realizations achieve the same rate as their FD counterparts and and therefore outperform existing hybrid designs.

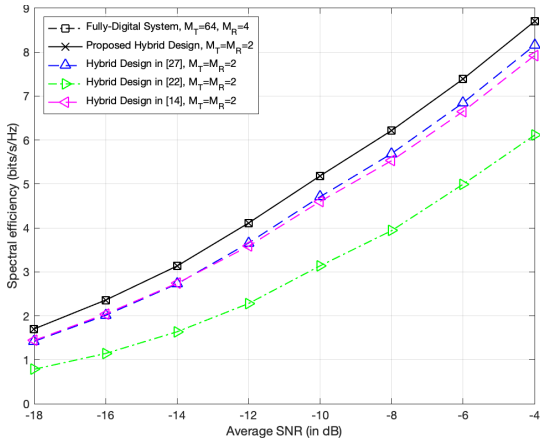


**FIGURE 15.** Spectral efficiency versus SNR of different methods for an downlink connection with $N_T = 64$ antenna massive-MIMO BS and a single user with $N_R = 4$.

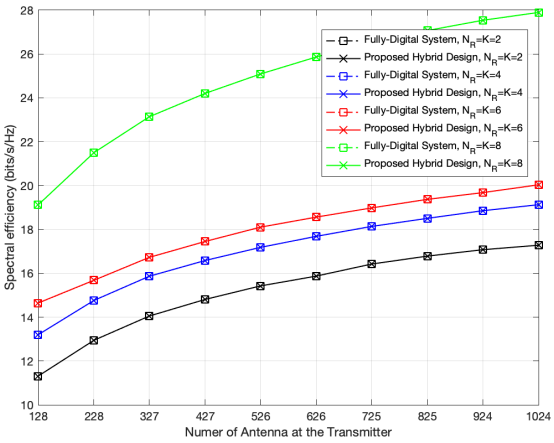


**FIGURE 16.** Spectral efficiency versus number of transmitter antennas for proposed and FD beamforming, with different numbers of receive antennas.

In order to evaluate the performance of the proposed ASP structure when number of antennas grows larger, simulations are performed for ultra-massive MIMO system configurations. Spectral efficiency versus number of transmitter antennas $N_T$ is plotted in Fig. 16 for different number of receive antennas. For the FD system the number of RF chains is equal to the number of transmitter antennas, i.e., $M_T = N_T$ whereas for the proposed hybrid structure the number of antennas is kept equal to the number of transmitted symbols, i.e., $M_T = K$. It can be seen that in all cases, the hybrid design with the proposed ASP architecture achieves the same performance as the corresponding FD system. For instance, for an ultra-massive MIMO transmitter with $N_T = 1024$ antennas and receiver with $M_T = 2$ antennas, the FD structure requires $N_R = 1024$ RF chains while the proposed structure guarantees the same performance with $M_T = 2$ RF chains.

### C. COMPUTATIONAL COMPLEXITY

The proposed ASP architecture is implemented with the same RF components as the conventional hybrid structures [13]–[21]. Moreover, since the constant unit modulus is not imposed on the entries for the resulting analog transformation matrix with our approach, the computational complexity of designing the analog and digital beamformers can be reduced. Compared to the FD system design, the additional computations required for the proposed ASP approach lie in the calculation of the phase-shifter parameters as given in (27). In the case of an eigen-mode FD beamformer for instance, the calculations in (27), in terms of complexity order, are dominated by the SVD and water filling algorithm needed for FD design, as represented by (31). Moreover, existing hybrid designs use sophisticated optimization or reconstruction techniques to handle the constant modulus constraint. For instance, the iterative algorithms in [14] and [27] require matrix inversion in each iteration. Consequently, the computational complexity of the proposed FD realizations with ASP is less than each iteration in these hybrid designs.

for proposed and FD, with different numbers of rece…

## VI. CONCLUSION

In this paper, we investigated the hybrid A/D structure as a general framework for signal processing in massive and ultra-massive-MIMO systems. We first explored the ASP network in details by developing a mathematical representation for any arbitrarily connected feed-forward ASP network comprised of phase-shifters, power-dividers and power combiners. Then, a novel ASP structure was proposed which is not bound to the unit modulus constraint. Subsequently, we focused on the transmitter and receiver sides by exploiting the newly proposed ASP architecture and generalizing generalizing the digital processing. Specifically, the optimization problem for the HSP beamformer was reformulated within the new representation framework, which facilitates its solution under a variety of constraints and requirements for the massive MIMO system. Finally simulation results were presented illustrating the superiority of the proposed architecture to the conventional hybrid designs for massive-MIMO systems.

## APPENDIX A

*Proof of Proposition 1:*

The matrix representation of the RF components in (8)-(10) are introduced such that the input and output signals can be of any size and thus can include RF branches that are not affected by the RF component. Consequently, we can sort the RF components such that the input of each RF component is the output of another RF component except for the first component. Let us denote the input and output of the $i^{th}$ RF component as $\mathbf{a}_i$ and $\mathbf{b}_i$, respectively. Consequently, we have $\mathbf{b}_{i-1} = \mathbf{a}_i$, $\mathbf{a}_1 = \mathbf{a}$ and $\mathbf{b} = \mathbf{b}_T$. To be more precise the following algorithm is used to assign the index $i$ for $i = 1, 2, \ldots, T$ to each RF element:

Note that step 1 has always an answer because of how $\mathbf{a}_i$ and $\mathbf{b}_i$ are defined. Moreover, it is possible that more than one RF component satisfy the condition in step 1.

**for** $i \leftarrow 1$ **to** $T$ **do**
  *1. Find an RF component whose input is* $\mathbf{a}_i$;
  *2. Assign index i to that RF component*;
  *3. Denote the output as* $\mathbf{b}_i$;
  *4.* $\mathbf{a}_{i+1} = \mathbf{b}_i$;
**end**

In these cases, the components are parallel, i.e, the signals are simultaneously entering them and any ordering of these components is acceptable. Now, for $i = 1, 2, \ldots, T$ we can write $\mathbf{b}_i$ in terms of $\mathbf{a}_i$. If the $i^{th}$ RF component is a phase-shifter, a power divider, or a power combiner, then we have $\mathbf{b}_i = \Phi(\gamma, \phi, \eta)\mathbf{P}_\pi \mathbf{a}_i$, $\mathbf{b}_i = \mathbf{Q}(\gamma, \mu, \eta)\mathbf{P}_\pi \mathbf{a}_i$, or $\mathbf{b}_i = \mathbf{Q}^t(\gamma, \mu, \eta)^t \mathbf{P}_\pi \mathbf{a}_i$, respectively. Note that, if the order of the signals is not changed before the $i^{th}$ component, we have $\mathbf{P}_\pi = \mathbf{I}$. Hence, the given ASP can be expressed as in (12). ■

## APPENDIX B

*Proof of Theorem 1:* By transposing (14) and (17), and the fact that the transpose of a permutation matrix is also a permutation matrix, we arrive at (13) and (16). The proofs for the remaining properties are presented below:

### 1) PROOF OF (13)

We show that for any vector $\mathbf{x}$ there exist $\pi'$ such that, if we have $\hat{\mathbf{x}}^{(1)} = \mathbf{Q}(\gamma, \mu, \eta)\mathbf{P}_\pi \mathbf{x}$ and $\hat{\mathbf{x}}^{(2)} = \mathbf{P}_{\pi'}\mathbf{Q}(\pi(\gamma), \mu, \eta)\mathbf{x}$ then $\hat{\mathbf{x}}^{(1)} = \hat{\mathbf{x}}^{(2)}$. By denoting $\mathbf{x}^{(\pi)} = \mathbf{P}_\pi \mathbf{x}$, we can write

$$\hat{\mathbf{x}}^{(1)} \overset{\pi}{=} [\mathbf{x}^{(\pi)^t}, x_\gamma^{(\pi)} \mathbf{1}_{\mu-1}^t]^t, \tag{57}$$

since $x_\gamma^{(\pi)} = x_{\pi(\gamma)}$ we can further write

$$\hat{\mathbf{x}}^{(1)} \overset{\pi}{=} [\mathbf{x}^t, x_{\pi(\gamma)} \mathbf{1}_{\mu-1}^t]^t. \tag{58}$$

On the other hand we can write

$$\mathbf{Q}\big(\pi(\gamma), \mu, \eta\big)\mathbf{x} \overset{\pi}{=} [\mathbf{x}^t, x_{\pi(\gamma)} \mathbf{1}_{\mu-1}^t]^t, \tag{59}$$

thus, we can conclude $\hat{\mathbf{x}}^{(1)} \overset{\pi}{=} \mathbf{Q}\big(\pi(\gamma), \mu, \eta\big)\mathbf{x}$; therefore, there exist $\mathbf{P}_{\pi'}$ such that $\hat{\mathbf{x}}^{(1)} = \hat{\mathbf{x}}^{(2)}$. ■

### 2) PROOF OF (15)

For $\gamma_1 < \gamma_2$ and $\gamma_1 > \gamma_2$, we show that $J = J' = 1$ and for $\gamma_1 = \gamma_2$ it will be shown that $J = \mu_1$ and $J' = \mu_2$. First, considering $\gamma_1 > \gamma_2$, we can write

$$\begin{aligned}&\mathbf{Q}(\gamma_1, \mu_1, \eta)\mathbf{Q}^t(\gamma_2, \mu_2, \eta)\\ &= \mathrm{bd}(\mathbf{I}_{\gamma_1-1}, \frac{1}{\sqrt{\mu_1}}\mathbf{1}_{\mu_1}, \mathbf{I}_{\eta-\gamma_1})\mathrm{bd}(\mathbf{I}_{\gamma_2-1}, \frac{1}{\sqrt{\mu_2}}\mathbf{1}_{\mu_2}^t, \mathbf{I}_{\eta-\gamma_2}).\end{aligned} \tag{60}$$

With simple matrix manipulation, we have

$$\begin{aligned}&\mathrm{bd}(\mathbf{I}_{\gamma_1-1}, \frac{1}{\sqrt{\mu_1}}\mathbf{1}_{\mu_1}, \mathbf{I}_{\eta-\gamma_1})\mathrm{bd}(\mathbf{I}_{\gamma_2-1}, \frac{1}{\sqrt{\mu_2}}\mathbf{1}_{\mu_2}^t, \mathbf{I}_{\eta-\gamma_2})\\ &= \mathrm{bd}(\mathbf{I}_{\gamma_2-1}, \frac{1}{\sqrt{\mu_2}}\mathbf{1}_{\mu_2}^t, \mathbf{I}_{\eta-\gamma_2+\mu_1-1})\mathrm{bd}\\ &\quad \times (\mathbf{I}_{\gamma_1-2+\mu_2}, \frac{1}{\sqrt{\mu_1}}\mathbf{1}_{\mu_1}, \mathbf{I}_{\eta-\gamma_1}),\end{aligned} \tag{61}$$

we can further write

$$\begin{aligned}&\mathrm{bd}(\mathbf{I}_{\gamma_2-1}, \frac{1}{\sqrt{\mu_2}}\mathbf{1}_{\mu_2}^t, \mathbf{I}_{\eta-\gamma_2+\mu_1-1})\mathrm{bd}\\ &\quad \times (\mathbf{I}_{\gamma_1-2+\mu_2}, \frac{1}{\sqrt{\mu_1}}\mathbf{1}_{\mu_1}, \mathbf{I}_{\eta-\gamma_1})\\ &= \mathbf{Q}^t(\gamma_2, \mu_2, \eta + \mu_1 - 1)\\ &\quad \times \mathbf{Q}(\gamma_1 + \mu_2 - 1, \mu_1, \eta + \mu_2 - 1).\end{aligned} \tag{62}$$

In case of $\gamma_1 < \gamma_2$, we can accordingly write

$$\begin{aligned}&\mathbf{Q}(\gamma_1, \mu_1, \eta)\mathbf{Q}^t(\gamma_2, \mu_2, \eta)\\ &= \mathrm{bd}(\mathbf{I}_{\gamma_1-1}, \frac{1}{\sqrt{\mu_1}}\mathbf{1}_{\mu_1}, \mathbf{I}_{\eta-\gamma_1})\mathrm{bd}(\mathbf{I}_{\gamma_2-1}, \frac{1}{\sqrt{\mu_2}}\mathbf{1}_{\mu_2}^t, \mathbf{I}_{\eta-\gamma_2}).\end{aligned} \tag{63}$$

Similar to (61), we have

$$\begin{aligned}&\mathrm{bd}(\mathbf{I}_{\gamma_1-1}, \frac{1}{\sqrt{\mu_1}}\mathbf{1}_{\mu_1}, \mathbf{I}_{\eta-\gamma_1})\mathrm{bd}(\mathbf{I}_{\gamma_2-1}, \frac{1}{\sqrt{\mu_2}}\mathbf{1}_{\mu_2}^t, \mathbf{I}_{\eta-\gamma_2})\\ &= \mathrm{bd}(\mathbf{I}_{\gamma_2+\mu_1-1}, \frac{1}{\sqrt{\mu_2}}\mathbf{1}_{\mu_2}^t, \mathbf{I}_{\eta+\mu_1-1})\mathrm{bd}\\ &\quad \times (\mathbf{I}_{\gamma_1-1}, \frac{1}{\sqrt{\mu_1}}\mathbf{1}_{\mu_1}, \mathbf{I}_{\eta+\mu_2-1}).\end{aligned} \tag{64}$$

We can then write

$$\begin{aligned}&\mathrm{bd}(\mathbf{I}_{\gamma_2+\mu_1-1}, \frac{1}{\sqrt{\mu_2}}\mathbf{1}_{\mu_2}^t, \mathbf{I}_{\eta+\mu_1-1})\mathrm{bd}\\ &\quad \times (\mathbf{I}_{\gamma_1-1}, \frac{1}{\sqrt{\mu_1}}\mathbf{1}_{\mu_1}, \mathbf{I}_{\eta+\mu_2-1})\\ &= \mathbf{Q}^t(\gamma_2 + \mu_1 - 1, \mu_2, \eta+\mu_1 - 1)\mathbf{Q}(\gamma_1, \mu_1, \eta + \mu_2 - 1).\end{aligned} \tag{65}$$

For $\gamma_1 = \gamma_2$, without loss of generality, we only provide the proof for $\gamma_1 = \gamma_2 = 1$ and $\eta = 1$, extending to other values of $\gamma_1$,$\gamma_2$ and $\eta$ straightforward but tedious. Hence, we show

$$\begin{aligned}\mathbf{Q}(1, \mu_1, 1)\mathbf{Q}^t(1, \mu_2, 1) &= \prod_{j=1}^{\mu_1} \mathbf{Q}^t(\gamma_j', \mu_j', \eta_j')\mathbf{P}_\pi\\ &\quad \times \prod_{j'=1}^{\mu_2} \mathbf{Q}(\gamma_{j'}'', \mu_{j'}'', \eta_{j'}'')\end{aligned} \tag{66}$$

The left hand side can be written as

$$\mathbf{Q}(1, \mu_1, 1)\mathbf{Q}^t(1, \mu_2, 1) = \frac{1}{\sqrt{\mu_1\mu_2}}\mathbf{1}_{\mu_1 \times \mu_2}. \tag{67}$$

Now, by letting $\gamma''_{j'} = (j'-1)\mu_1 + 1$, $\mu''_{j'} = \mu_1$ and $\eta''_{j'} = (j'-1)\mu_1 + \mu_2 - j' + 1$, we have

$$\prod_{j'=1}^{\mu_2} \mathbf{Q}\big((j'-1)\mu_1+1, \mu_1, (j'-1)\mu_1+\mu_2-j'+1\big) = \mathbf{I}_{\mu_2} \otimes \frac{1}{\sqrt{\mu_1}}\mathbf{1}_{\mu_1}. \tag{68}$$

We can then form the permutation matrix $\mathbf{P}_\pi$ with

$$\pi_i = \lceil i/\mu_1 \rceil + \mu_2\big((i-1) \bmod (\mu_1)\big), \tag{69}$$

which results in

$$\mathbf{P}_{\pi_i}\big(\mathbf{I}_{\mu_2} \otimes \mathbf{1}_{\mu_1}\big) = \mathbf{1}_{\mu_1} \otimes \mathbf{I}_{\mu_2}. \tag{70}$$

Then by letting $\gamma'_j = j$, $\mu'_j = \mu_1$ and $\eta'_j = (\mu_2 - j)\mu_1 + j$, we arrive at

$$\prod_{j=1}^{\mu_1} \mathbf{Q}\big(j, \mu_2, (\mu_1-j)\mu_2 + j\big) = \mathbf{I}_{\mu_1} \otimes \frac{1}{\sqrt{\mu_2}}\mathbf{1}^t_{\mu_2}. \tag{71}$$

From the above equation, (68) and (70), we can write

$$\prod_{j=1}^{\mu_1} \mathbf{Q}^t(\gamma'_j, \mu'_j, \eta'_j)\mathbf{P}_\pi \prod_{j'=1}^{\mu_2} \mathbf{Q}(\gamma''_{j'}, \mu''_{j'}, \eta''_{j'}) = \frac{1}{\sqrt{\mu_1\mu_2}}\big(\mathbf{I}_{\mu_1} \otimes \mathbf{1}^t_{\mu_2}\big)\big(\mathbf{1}_{\mu_1} \otimes \mathbf{I}_{\mu_2}\big). \tag{72}$$

The right hand side of the above equation can be further simplified as

$$\big(\mathbf{I}_{\mu_1} \otimes \mathbf{1}^t_{\mu_2}\big)\big(\mathbf{1}_{\mu_1} \otimes \mathbf{I}_{\mu_2}\big) = \mathbf{1}_{\mu_1 \times \mu_2}, \tag{73}$$

which can be easily verified by invoking the mixed-product property.[2] Consequently, using the above equation,(72) and (67), we showed (66) is held which concludes the proof. ■

### 3) PROOF OF (16)

For $\gamma_1 > \gamma_2$, and $\gamma_1 < \gamma_2$,

$$\prod_{j=1}^{J} \Phi(\gamma'_j, \phi'_j, \eta'_j)\mathbf{Q}(\gamma_1, \mu, \eta) = \mathbf{Q}(\gamma_1, \mu, \eta)\Phi(\gamma_2, \phi, \eta), \tag{74}$$

is actually simplified to the case where $J$ is equal to one. Thus, for $\gamma_1 > \gamma_2$ one can easily check

$$\Phi(\gamma_2, \phi, \eta + \mu - 1)\mathbf{Q}(\gamma_1, \mu, \eta) = \mathbf{Q}(\gamma_1, \mu, \eta)\Phi(\gamma_2, \phi, \eta). \tag{75}$$

Similarly, for $\gamma_1 < \gamma_2$, we can write

$$\Phi(\gamma_2, \phi, \eta + \mu - 1)\mathbf{Q}(\gamma_1, \mu, \eta) = \mathbf{Q}(\gamma_1, \mu, \eta)\Phi(\gamma_2, \phi, \eta). \tag{76}$$

[2] If $\mathbf{A}$,$\mathbf{B}$,$\mathbf{C}$ and $\mathbf{D}$ are matrices of appropriate sizes, then $(\mathbf{A}\otimes\mathbf{b})(\mathbf{C}\otimes\mathbf{D}) = (\mathbf{AC}) \otimes (\mathbf{BD})$.

In case of $\gamma_1 = \gamma_2$, $J = \mu$ and we can write

$$\prod_{j=1}^{\mu} \Phi(\gamma_1 + j - 1, \phi, \eta + \mu - 1)\mathbf{Q}(\gamma_1, \mu, \eta) = \mathbf{Q}(\gamma_1, \mu, \eta)\Phi(\gamma_1, \phi, \eta). \tag{77}$$

which can be easily verified by matrix manipulations. ■

## APPENDIX C

### 4) PROOF OF (18)

To show that $\mathbf{E_v}$ is a diagonal matrix, we can use induction and the fact that for a diagonal matrix $\mathbf{D}$ and permutation matrix $\mathbf{P}_\pi$, the matrix $\hat{\mathbf{D}} = \mathbf{P}_\pi \mathbf{D} \mathbf{P}_\pi{}^t$ is also a diagonal matrix. For $J = 1$ the statement is true, and we must prove for $J = K + 1$ we have:

$$\hat{\mathbf{E}}_\mathbf{v}\hat{\mathbf{P}}_\pi = \prod_{j=1}^{K+1} \Phi(\gamma_j, \phi_j, N_\mathbf{p})\mathbf{P}_{\pi_j}. \tag{78}$$

By assuming for $J = K$, matrix $\mathbf{E_v}$ is diagonal and $\mathbf{P}_\pi$ is a permutation matrix, we can rewrite the above equation as

$$\hat{\mathbf{E}}_\mathbf{v}\hat{\mathbf{P}}_\pi = \mathbf{E_v}\mathbf{P}_\pi \Phi(\gamma_{K+1}, \phi_{K+1}, N_\mathbf{p})\mathbf{P}_{\pi_{K+1}}. \tag{79}$$

We can therefore write

$$\hat{\mathbf{E}}_\mathbf{v}\hat{\mathbf{P}}_\pi = \mathbf{E_v}\mathbf{P}_\pi \Phi(\gamma_{K+1}, \phi_{K+1}, N_\mathbf{p})\mathbf{P}^t_\pi\mathbf{P}_\pi\mathbf{P}_{\pi_{K+1}}. \tag{80}$$

Using the aforementioned property of permutation matrices, we know $\hat{\Phi} = \mathbf{P}_\pi \Phi(\gamma_{K+1}, \phi_{K+1}, N_\mathbf{p})\mathbf{P}^t_\pi$ is a diagonal matrix. We further know that $\hat{\mathbf{P}}_\pi = \mathbf{P}_\pi\mathbf{P}_{\pi_{K+1}}$ is a permutation matrix thus we can write:

$$\hat{\mathbf{E}}_\mathbf{v}\hat{\mathbf{P}}_\pi = \mathbf{E_v}\hat{\Phi}\hat{\mathbf{P}}_\pi. \tag{81}$$

Since $\mathbf{E_v}$ and $\hat{\Phi}$ are both diagonal so is $\hat{\mathbf{E}}_\mathbf{v}$. Furthermore, since all the diagonal entries are unit modulo complex numbers their products are also on the unit circle and thus $\mathbf{v} = [e^{j\phi_1}, e^{j\phi_2}, \ldots, e^{j\phi_{N_\mathbf{p}}}]^t \in \mathbb{U}^{N_\phi}$. ■

### 5) PROOF OF (20)

Induction can be used to prove this statement. For $J = 1$, one can easily find $\mathbf{P}_{\pi'_1}$ such that

$$\mathbf{P}^t_{\pi'_1}\mathrm{bd}(\mathbf{I}_{\gamma-1}, \frac{1}{\sqrt{\mu}}\mathbf{1}_\mu, \mathbf{I}_{\eta-\gamma}) = \begin{bmatrix} 0 & \frac{1}{\sqrt{\mu}}\mathbf{1}_\mu & 0 \\ \mathbf{I}_{\gamma-1} & 0 & 0 \\ 0 & 0 & \mathbf{I}_{\eta-\gamma} \end{bmatrix}, \tag{82}$$

accordingly there exist $\mathbf{P}_{\pi'_2}$ such that

$$\mathbf{P}^t_{\pi'_1}\mathrm{bd}(\mathbf{I}_{\gamma-1}, \frac{1}{\sqrt{\mu}}\mathbf{1}_\mu, \mathbf{I}_{\eta-\gamma})\mathbf{P}^t_{\pi'_2} = \begin{bmatrix} \frac{1}{\sqrt{\mu}}\mathbf{1}_\mu & 0 & 0 \\ 0 & \mathbf{I}_{\gamma-1} & 0 \\ 0 & 0 & \mathbf{I}_{\eta-\gamma} \end{bmatrix}, \tag{83}$$

using the fact that permutation matrices are orthogonal, we can write $\mathbf{Q}(1, \mu, \eta) = \mathbf{P}_{\pi'_1}\mathrm{bd}(\frac{1}{\sqrt{\mu}}\mathbf{1}_\mu, \mathbf{I}_\eta)\mathbf{P}_{\pi'_2}$. Now, let

us assume for $J = K$ we have:

$$\prod_{j=1}^{K} \mathbf{Q}(\gamma_j, \mu_j, \eta_j) = \mathbf{P}_\pi \mathbf{D_d} \mathbf{P}_{\pi'}, \tag{84}$$

We can thus write the following for $J = K + 1$

$$\prod_{j=1}^{K+1} \mathbf{Q}(\gamma_j, \mu_j, \eta_j) = \mathbf{P}_\pi \mathbf{D_d} \mathbf{P}_{\pi'} \mathbf{Q}(\gamma_{K+1}, \mu_{K+1}, \eta_{K+1}). \tag{85}$$

According to the $J = 1$ case, there exist $\mathbf{P}_{\pi_3'}$ and $\mathbf{P}_{\pi_4'}$ such that

$$\mathbf{Q}(\gamma_{K+1}, \mu_{K+1}, \eta_{K+1}) = \mathbf{P}_{\pi_3'} \mathrm{bd}(\frac{1}{\sqrt{\mu_{K+1}}} \mathbf{1}_{\mu_{K+1}}, \mathbf{I}) \mathbf{P}_{\pi_4'}, \tag{86}$$

thus,

$$\prod_{j=1}^{K+1} \mathbf{Q}(\gamma_j, \mu_j, \eta_j) = \mathbf{P}_\pi \mathbf{D_d} \mathbf{P}_{\pi'} \mathbf{P}_{\pi_3'} \mathrm{bd}(\frac{1}{\sqrt{\mu_{K+1}}} \mathbf{1}_{\mu_{K+1}}, \mathbf{I}) \mathbf{P}_{\pi_4'}. \tag{87}$$

Let us first define $\mathbf{P}_{\pi_5'} = \mathbf{P}_{\pi'} \mathbf{P}_{\pi_3'}$, then by considering $\mathbf{D_d} \mathbf{P}_{\pi_5'}$, the permutation matrix $\mathbf{P}_{\pi_5'}$ rearranges the columns of $\mathbf{D_d}$. Therefore, there exist permutation matrix $\mathbf{P}_{\pi_6'}$ that rearranges the rows of $\mathbf{D_d} \mathbf{P}_{\pi_5'}$ to make a block diagonal matrix

$$\mathbf{P}^t_{\pi_6'} \mathbf{D_d} \mathbf{P}_{\pi_5'} = \mathbf{D_{d'}}, \tag{88}$$

where $\mathbf{D_{d'}} = \mathrm{bd}(\frac{1}{\sqrt{\delta_1'}} \mathbf{1}_{\delta_1'}, \frac{1}{\sqrt{\delta_2'}} \mathbf{1}_{\delta_2'}, \ldots, \frac{1}{\sqrt{\delta_{N_d}'}} \mathbf{1}_{\delta_{N_d}'})$. It is possible that $\delta_i' = 1$ for individual $i$ or some consecutive number indices which result it diagonal block of identity matrices $\mathbf{I}$. From (87) and (88), we arrive at

$$\begin{aligned} &\mathbf{P}_\pi \mathbf{D_d} \mathbf{P}_{\pi'} \mathbf{Q}_{(\gamma_{K+1}, \mu_{K+1}, \eta_{K+1})} \\ &\quad = \mathbf{P}_\pi \mathbf{P}_{\pi_6'} \mathbf{D_{d'}} \mathrm{bd}(\frac{1}{\sqrt{\mu_{K+1}}} \mathbf{1}_{\mu_{K+1}}, \mathbf{I}) \mathbf{P}_{\pi_4'}. \end{aligned} \tag{89}$$

The above equation can be further simplified as $\mathbf{D_{d'}} \mathrm{bd}(\frac{1}{\sqrt{\mu_{K+1}}} \mathbf{1}_{\mu_{K+1}}, \mathbf{I}) = \mathbf{D_{d''}}$ where $\mathbf{D_{d''}} = \mathrm{bd}(\frac{1}{\sqrt{\delta_1' + \mu_{K+1}}} \mathbf{1}_{\delta_1' + \mu_{K+1}}, \frac{1}{\sqrt{\delta_2'}} \mathbf{1}_{\delta_2'}, \ldots, \frac{1}{\sqrt{\delta_{N_d}'}} \mathbf{1}_{\delta_{N_d}'})$. Therefore by defining $\mathbf{P}_{\pi_7'} = \mathbf{P}_\pi \mathbf{P}_{\pi_6'}$, and from (85) and (89) we have

$$\prod_{j=1}^{K+1} \mathbf{Q}(\gamma_j, \mu_j, \eta_j) = \mathbf{P}_{\pi_7'} \mathbf{D_{d''}} \mathbf{P}_{\pi_4'}, \tag{90}$$

which proves the statement. ■

### 6) PROOF OF (22)

For $J = 1$, we have to show that $\mathbf{C_d}$ has the block diagonal structure of (23) in $\mathbf{P}_\pi \mathbf{C_d} \mathbf{P}_{\pi'} = \mathbf{Q}^t(\gamma, \mu, \eta) \mathbf{P}_{\pi_1}$. According to (83), we can write $\mathbf{Q}^t(\gamma, \mu, \eta) \mathbf{P}_{\pi_1} = \mathbf{P}_\pi \mathrm{bd}(\frac{1}{\sqrt{\mu}} \mathbf{1}_\mu, \mathbf{I}) \mathbf{P}_{\pi'} \mathbf{P}_{\pi_1}$. Since the product of two permutation matrices is also a permutation matrix, we have: $\mathbf{P}_{\pi'} = \mathbf{P}_{\pi'} \mathbf{P}_{\pi_1}$. To continue the proof with induction, we assume that for $J = K$ there exist $\mathbf{P}_\pi$,$\mathbf{P}_{\pi'}$ and $\mathbf{C_d}$ such that $\mathbf{P}_\pi \mathbf{C_d} \mathbf{P}_{\pi'} = \prod_{j=1}^{J} \mathbf{Q}^t(\gamma_j, \mu_j, \eta_j) \mathbf{P}_{\pi_j}$. Now, for $J = K + 1$ we can write:

$$\prod_{j=1}^{K+1} \mathbf{Q}^t(\gamma_j, \mu_j, \eta_j) \mathbf{P}_{\pi_j} = \mathbf{Q}^t(\gamma_1, \mu_1, \eta_1) \mathbf{P}_{\pi_1} \mathbf{P}_\pi \mathbf{C_d} \mathbf{P}_{\pi'}. \tag{91}$$

According to the $J = 1$ case, there exist $\mathbf{P}_{\pi_1'}$ and $\mathbf{P}_{\pi_2'}$ such that

$$\mathbf{Q}^t(\gamma_1, \mu_1, \eta_1) = \mathbf{P}_{\pi_1'} \mathrm{bd}(\frac{1}{\sqrt{\mu_1}} \mathbf{1}_{\mu_1}, \mathbf{I}) \mathbf{P}_{\pi_2'}, \tag{92}$$

Be defining a new permutation matrix $\mathbf{P}_{\pi_3'} = \mathbf{P}_{\pi_2} \mathbf{P}_{\pi_1} \mathbf{P}_\pi$, we can write the left hand-side of (91) as:

$$\mathbf{Q}^t(\gamma_1, \mu_1, \eta_1) \mathbf{P}_{\pi_1} \mathbf{P}_\pi \mathbf{C_d} \mathbf{P}_{\pi'} = \mathbf{P}_{\pi_1'} \mathrm{bd}(\frac{1}{\sqrt{\mu_1}} \mathbf{1}_{\mu_1}, \mathbf{I}) \mathbf{P}_{\pi_3'} \mathbf{C_d} \mathbf{P}_{\pi'}. \tag{93}$$

Considering $\mathbf{P}_{\pi_3'} \mathbf{C_d}$, permutation matrix $\mathbf{P}_{\pi_3'}$ rearranges the rows of $\mathbf{C_d}$. Therefore, there exist permutation matrix $\mathbf{P}_{\pi_4'}$ that rearranges the columns of $\mathbf{P}_{\pi_3'} \mathbf{C_d}$ to make a block diagonal matrix

$$\mathbf{P}_{\pi_3'} \mathbf{C_d} \mathbf{P}_{\pi_4'} = \mathbf{C_{d'}}, \tag{94}$$

where $\mathbf{C_{d'}} = \mathrm{bd}(\frac{1}{\sqrt{\delta_1'}} \mathbf{1}^t_{\delta_1'}, \frac{1}{\sqrt{\delta_2'}} \mathbf{1}^t_{\delta_2'}, \ldots, \frac{1}{\sqrt{\delta_{M_c}'}} \mathbf{1}^t_{\delta_{M_c}'})$. Note that it is possible that $\delta_i' = 1$ for individual $i$ or some consecutive number indices which result it diagonal block of identity matrices $\mathbf{I}$. From (93), (94) and the fact that $\mathbf{P}_{\pi_4'} \mathbf{P}^t_{\pi_4'}$, we can write

$$\begin{aligned} &\mathbf{P}_{\pi_1'} \mathrm{bd}(\frac{1}{\sqrt{\mu_1}} \mathbf{1}_{\mu_1}, \mathbf{I}) \mathbf{P}_{\pi_3'} \mathbf{C_d} \mathbf{P}_{\pi'} \\ &\quad = \mathbf{P}_{\pi_1'} \mathrm{bd}(\frac{1}{\sqrt{\mu_1}} \mathbf{1}_{\mu_1}, \mathbf{I}) \mathbf{C_{d'}} \mathbf{P}^t_{\pi_4'} \mathbf{P}_{\pi'}. \end{aligned} \tag{95}$$

To further simplify the above equation, we can write $\mathrm{bd}(\frac{1}{\sqrt{\mu_1}} \mathbf{1}_{\mu_1}, \mathbf{I}) \mathbf{C_{d'}} = \mathbf{C_{d''}}$ where

$$\delta_i'' = \begin{cases} \sum_{j=1}^{\mu_1} \delta_j', & i = 1 \\ \delta'_{(i-1+\mu_1)}, & \text{otherwise} \end{cases}. \tag{96}$$

To take the last step, there exist permutation matrices $\mathbf{P}_{\pi_5'}$ and $\mathbf{P}_{\pi_6'}$ such that $\mathbf{P}^t_{\pi_5'} \mathbf{C_{d''}} \mathbf{P}^t_{\pi_6'} = \mathbf{C_{d'''}}$ where for some $L$, we can have

$$\mathbf{C_{d'''}} = \mathrm{bd}(\frac{1}{\sqrt{\delta_1}} \mathbf{1}^t_{\delta_1}, \frac{1}{\sqrt{\delta_2}} \mathbf{1}^t_{\delta_2}, \ldots, \frac{1}{\sqrt{\delta_L}} \mathbf{1}^t_{\delta_L}, \mathbf{I}). \tag{97}$$

From the above equation and (95) we have

$$\mathbf{P}_{\pi_1'} \mathrm{bd}(\frac{1}{\sqrt{\mu_1}} \mathbf{1}_{\mu_1}, \mathbf{I}) \mathbf{P}_{\pi_3'} \mathbf{C_d} \mathbf{P}_{\pi'} = \mathbf{P}_{\pi_1'} \mathbf{P}_{\pi_5'} \mathbf{C_{d'''}} \mathbf{P}_{\pi_6'} \mathbf{P}^t_{\pi_4'} \mathbf{P}_{\pi'}. \tag{98}$$

Now by defining permutation matrices $\mathbf{P}_{\pi_7'} = \mathbf{P}_{\pi_1'} \mathbf{P}_{\pi_5'}$, $\mathbf{P}_{\pi_8'} = \mathbf{P}_{\pi_6'} \mathbf{P}^t_{\pi_4'} \mathbf{P}_{\pi'}$ and from (91) to (98), we arrive at

$$\prod_{j=1}^{K+1} \mathbf{Q}^t(\gamma_j, \mu_j, \eta_j) \mathbf{P}_{\pi_j} = \mathbf{P}_{\pi_7'} \mathbf{C_{d'''}} \mathbf{P}_{\pi_8'}, \tag{99}$$

which proves the statement. ■

## APPENDIX D

*Proof of Theorem 2:* Without loss of generality, let us assume there are a total of $T$ RF components, i.e., $P$ combiners, $R$ dividers repectively, and $Q$ phase-shifters, so that $T = P + Q + R$. According to properties (14), (15) and (17) in Theorem 1, we can rewrite (12) as follows by commuting the combiner matrices to the left hand side, i.e,

$$\prod_{i=1}^{T}\mathbf{A}_{u_i}(\theta_i)=\prod_{j=1}^{P}\mathbf{Q}^t(\theta_j)\prod_{i=1}^{T'}\mathbf{A}_{u_i}(\theta_i), \tag{100}$$

where $T' = T - P$. Similarly, the divider matrices can be moved to the right hand side using properties (13), (15) and (17), thus,

$$\prod_{i=1}^{T}\mathbf{A}_{u_i}(\theta_i)=\prod_{j=1}^{P}\mathbf{Q}^t(\theta_j)\prod_{i=1}^{T''}\mathbf{A}_{u_i}(\theta_i)\prod_{k=1}^{R}\mathbf{Q}(\theta_k), \tag{101}$$

where $T'' = T-P-R$. In (101) only the permutation and single phase-shifter matrices are in the middle of the expression. Therefore, without loss of generality and due to the fact that permutation and single phase-shifter matrices can be identity matrices we can write: $\prod_{i=1}^{T''}\mathbf{A}_{u_i}(\theta_i) = \prod_{i=1}^{J}\Phi(\gamma_i,\phi_i,\eta_i)\mathbf{P}_{\pi_i}$, hence,

$$\prod_{i=1}^{T}\mathbf{A}_{u_i}(\theta_i)=\prod_{j=1}^{P}\mathbf{Q}^t(\theta_j)\prod_{i=1}^{Q}\Phi(\gamma_i,\phi_i,\eta_i)\mathbf{P}_{\pi_i}\prod_{j=k}^{R}\mathbf{Q}(\theta_k). \tag{102}$$

Now, using (18), (20), (22), and the fact that product of permutation matrices is another permutation matrix, we have

$$\prod_{i=1}^{T}\mathbf{A}_{u_i}(\theta_i)=\mathbf{P}_{\pi_1}\mathbf{C}_{\mathbf{d}}\mathbf{P}_{\pi_2}\mathbf{E}_{\mathbf{v}}\mathbf{P}_{\pi_3}\mathbf{D}_{\hat{\mathbf{d}}}\mathbf{P}_{\pi_4}, \tag{103}$$

which follows,

$$\mathbf{b}=\mathbf{P}_{\pi_1}\mathbf{C}_{\mathbf{d}}\mathbf{P}_{\pi_2}\mathbf{E}_{\mathbf{v}}\mathbf{P}_{\pi_3}\mathbf{D}_{\hat{\mathbf{d}}}\mathbf{P}_{\pi_4}\mathbf{a}. \tag{104}$$

By defining

$$\begin{aligned}&\mathbf{b}=\mathbf{P}_{\pi_1}\mathbf{h}^{(1)},\quad \mathbf{h}^{(1)}=\mathbf{C}_{\mathbf{d}}\mathbf{h}^{(2)},\quad \mathbf{h}^{(2)}=\mathbf{P}_{\pi_2}\mathbf{h}^{(3)},\\ &\mathbf{h}^{(3)}=\mathbf{E}_{\mathbf{v}}\mathbf{h}^{(4)},\quad \mathbf{h}^{(4)}=\mathbf{P}_{\pi_3}\mathbf{h}^{(5)},\quad \mathbf{h}^{(5)}=\mathbf{D}_{\hat{\mathbf{v}}}\mathbf{h}^{(6)},\\ &\mathbf{h}^{(6)}=\mathbf{P}_{\pi_4}\mathbf{a},\end{aligned} \tag{105}$$

we can further have

$$\begin{aligned}&b_i=h^{(1)}_{\pi_1^{-1}(i)},\qquad h^{(1)}_i=\frac{1}{\sqrt{\delta_i}}\sum_{j=\psi_\delta(i-1)+1}^{\psi_\delta(i)}h^{(2)}_j,\\ &h^{(2)}_i=h^{(3)}_{\pi_2^{-1}(i)},\qquad h^{(3)}_i=e^{j\phi_i}h^{(4)}_i\\ &h^{(4)}_i=h^{(5)}_{\pi_3^{-1}(i)},\qquad h^{(5)}_i=\frac{1}{\sqrt{\hat{\delta}_{\varphi_{\hat{\delta}}(i)}}}h^{(6)}_{\varphi_{\hat{\delta}}(i)},\\ &h^{(6)}_i=a_{\pi_4^{-1}(i)},\end{aligned} \tag{106}$$

where $\psi_\delta(i)=\sum_{k=1}^{i}\delta_k$ and $\varphi_{\hat{\delta}}(i)=\{j\in\mathbb{N}|\psi_{\hat{\delta}}(j-1)\le i\le\psi_{\hat{\delta}}(j)\}$. Consequently, we arrive at (107) presented at the top of the next page, where by defining

$$u_{i,j}=\pi_2^{-1}\Big(\psi_\delta\big(\pi_1^{-1}(i)-1\big)+j\Big), \tag{108}$$

$$\dot{v}(n)=\varphi_{\hat{\delta}}\big(\pi_3^{-1}(n)\big), \tag{109}$$

$$\ddot{v}(n)=\pi_4^{-1}(\dot{v}(n)), \tag{110}$$

we can write

$$b_i=\frac{1}{\sqrt{\delta_{\pi_1^{-1}(i)}}}\sum_{j=1}^{\delta_{\pi_1^{-1}(i)}}\frac{a_{\ddot{v}(\dot{v}(u_{(i,j)}))}}{\sqrt{\hat{\delta}_{\dot{v}(u_{(i,j)})}}}\exp\{j\phi_{u_{(i,j)}}\}. \tag{111}$$

Without loss of generality, we can further have

$$b_i=\frac{1}{\sqrt{\delta_{\pi_1^{-1}(i)}}}\sum_{k=1}^{M}a_k\Big(\frac{1}{\sqrt{\hat{\delta}_{k'}}}\Big(\sum_{<\dot{v}(u_{(i,j)})=k'>}e^{j\phi_{u_{(i,j)}}}\Big)\Big), \tag{112}$$

for $\ddot{v}(k')=k$. By defining $\hat{\delta}'_k=\hat{\delta}_{k'}$ and $\phi'_{k,l}=\phi_{u_{(i,j)}}$ for $\ddot{v}(\dot{v}(u_{(i,j)}))=k$ we can write

$$b_i=\frac{1}{\sqrt{\delta_{\pi_1^{-1}(i)}}}\sum_{k=1}^{M}\frac{1}{\sqrt{\hat{\delta}'_k}}a_k\Big(\sum_{l=1}^{L_k}e^{j\phi'_{k,l}}\Big). \tag{113}$$

Since in $\sum_{l=1}^{L_k}e^{j\phi'_{k,l}}$ by adding even number of phase-shifters which can cancel each other ($e^{j2\pi}$ and $e^{j\pi}$) the sum remains the same, we can have $L_k = L$. Furthermore, we can write

$$\begin{aligned}&\delta_{\pi_1^{-1}(i)}=LM,\\ &\hat{\delta}'_k=LN,\end{aligned} \tag{114}$$

hence,

$$b_i=\frac{1}{\sqrt{MN}}\sum_{k=1}^{M}a_k\Big(\sum_{l=1}^{L}\frac{e^{j\phi'_{k,l}}}{L}\Big). \tag{115}$$

From Lemma 1 in Appendix E we can write:

$$b_i=\frac{1}{\sqrt{MN}}\sum_{k=1}^{M}z_{k,i}a_k. \tag{116}$$

Thus, we arrive at

$$\mathbf{b}=\frac{1}{\sqrt{MN}}\mathbf{A}\mathbf{a}. \tag{117}$$

## APPENDIX E

*Lemma 1:* For arbitrary $\theta_l \in [0, 2\pi]$ where $l = 1, 2, \ldots, L$, if we have $z=\sum_{l=1}^{L}\frac{e^{j\theta_l}}{L}$, then $0\le|z|\le 1$.

*Proof:* The proof follows from successive applications of the triangle inequality in complex plane as $0 \le |\sum_{l=1}^{L}e^{j\theta_l}| \le L$. ■

*Lemma 2:* Any complex number $z$ where $0\le|z|\le L$ for $L \ge 2$ can be written as: $z=\sum_{l=1}^{\bar{L}}e^{j\theta_l}$ where $\bar{L} = L + (L \bmod 2)$, $\theta_l \in [0, 2\pi]$ and $\theta_l$'s may be non-unique.

$$b_i = \delta^{-1/2}_{\pi_1^{-1}(i)} \sum_{j=\psi_\delta(\pi_1^{-1}(i)-1)+1}^{\psi_\delta(\pi_1^{-1}(i))} \hat{\delta}^{-1/2}_{\varphi_{\hat{\delta}}(\pi_3^{-1}(\pi_2^{-1}(j)))} \exp\{j\phi_{\pi_2^{-1}(j)}\} a_{\pi_4^{-1}(\varphi_{\hat{\delta}}(\pi_3^{-1}(\pi_2^{-1}(j))))}, \tag{107}$$

*Proof:* The proof for $L = 2$ is presented in [15], thus, for a given $0 \leq |z'| \leq 2$ we have $z' = e^{j\theta_1} + e^{j\theta_2}$. Thus, it is sufficient to provide the proof for $L = 2L'$ and then $L = 2L' + 1$ when $L \geq 2$.

For $L = 2L'$: We have $\bar{L} = 2L'$, thus, we can write $z = L'z'$ where $0 \leq |z'| \leq 2$. Therefore, we can similarly write $z = L'(e^{j\theta_1} + e^{j\theta_2}) = L'e^{j\theta_1} + L'e^{j\theta_2}$. Then by writing $L'e^{j\theta_1} = \sum_{l=1}^{L'} e^{j\theta_1}$ and $L'e^{j\theta_2} = \sum_{l=1}^{L'} e^{j\theta_2}$ we can write $z = \sum_{l=1}^{L'} e^{j\theta_1} + \sum_{l=1}^{L'} e^{j\theta_2}$ which follows $z = \sum_{l=1}^{2L'} e^{j\theta'_l}$ where $\theta'_l = \theta_1$ for $l = 1, 2, \ldots, L'$ and $\theta'_l = \theta_2$ for $l = L'+1, \ldots, L$.

For $L = 2L' + 1$: We have $\bar{L} = 2(L' + 1)$, thus from the above case there exist $\theta'_l$'s such that $z = \sum_{l=1}^{2(L'+1)} e^{j\theta'_l}$. ■

## REFERENCES


[1] R. C. Daniels and R. W. Heath, Jr., "60 GHz wireless communications: Emerging requirements and design recommendations," *IEEE Veh. Technol. Mag.*, vol. 2, no. 3, pp. 41–50, Sep. 2007.

[2] F. Rusek, D. Persson, B. Kiong Lau, E. G. Larsson, T. L. Marzetta, and F. Tufvesson, "Scaling up MIMO: Opportunities and challenges with very large arrays," *IEEE Signal Process. Mag.*, vol. 30, no. 1, pp. 40–60, Jan. 2013.

[3] E. G. Larsson, O. Edfors, F. Tufvesson, and T. L. Marzetta, "Massive MIMO for next generation wireless systems," *IEEE Commun. Mag.*, vol. 52, no. 2, pp. 186–195, Feb. 2014.

[4] I. F. Akyildiz, C. Han, and S. Nie, "Combating the distance problem in the millimeter wave and terahertz frequency bands," *IEEE Commun. Mag.*, vol. 56, no. 6, pp. 102–108, Jun. 2018.

[5] E. Björnson, L. Sanguinetti, H. Wymeersch, J. Hoydis, and T. L. Marzetta, "Massive MIMO is a reality—What is next?: Five promising research directions for antenna arrays," *Digit. Signal Process.*, vol. 94, pp. 3–20, Jun. 2019, doi: 10.1016/j.dsp.2019.06.007.

[6] S. A. Busari, K. M. S. Huq, S. Mumtaz, J. Rodriguez, Y. Fang, D. C. Sicker, S. Al-Rubaye, and A. Tsourdos, "Generalized hybrid beamforming for vehicular connectivity using THz massive MIMO," *IEEE Trans. Veh. Technol.*, vol. 68, no. 9, pp. 8372–8383, Sep. 2019.

[7] S. A. Busari, K. M. S. Huq, S. Mumtaz, L. Dai, and J. Rodriguez, "Millimeter-wave massive MIMO communication for future wireless systems: A survey," *IEEE Commun. Surveys Tuts.*, vol. 20, no. 2, pp. 836–869, 2nd Quart., 2018.

[8] X. Zhang, A. F. Molisch, and S.-Y. Kung, "Variable-phase-shift-based RF-baseband codesign for MIMO antenna selection," *IEEE Trans. Signal Process.*, vol. 53, no. 11, pp. 4091–4103, Nov. 2005.

[9] A. Alkhateeb, J. Mo, N. Gonzalez-Prelcic, and R. W. Heath, Jr., "MIMO precoding and combining solutions for millimeter-wave systems," *IEEE Commun. Mag.*, vol. 52, no. 12, pp. 122–131, Dec. 2014.

[10] A. Morsali, S. Saleh Hosseini, B. Champagne, and X.-W. Chang, "Design criteria for omnidirectional STBC in massive MIMO systems," *IEEE Wireless Commun. Lett.*, vol. 8, no. 5, pp. 1435–1439, Oct. 2019.

[11] F. Koroupi, A. Morsali, V. Niktab, M. Shahabinejad, and S. Talebi, "Quasi-orthogonal space–frequency and space–time–frequency block codes with modified performance and simplified decoder," *IET Commun.*, vol. 11, no. 11, pp. 1655–1661, Aug. 2017.

[12] M. Samavat, A. Morsali, and S. Talebi, "Delay–interleaved cooperative relay networks," *IEEE Commun. Lett.*, vol. 18, no. 12, pp. 2137–2140, Dec. 2014.

[13] O. E. Ayach, S. Rajagopal, S. Abu-Surra, Z. Pi, and R. W. Heath, Jr., "Spatially sparse precoding in millimeter wave MIMO systems," *IEEE Trans. Wireless Commun.*, vol. 13, no. 3, pp. 1499–1513, Mar. 2014.

[14] F. Sohrabi and W. Yu, "Hybrid digital and analog beamforming design for large-scale antenna arrays," *IEEE J. Sel. Topics Signal Process.*, vol. 10, no. 3, pp. 501–513, Apr. 2016.

[15] T. E. Bogale, L. B. Le, A. Haghighat, and L. Vandendorpe, "On the number of RF chains and phase shifters, and scheduling design with hybrid analog–digital beamforming," *IEEE Trans. Wireless Commun.*, vol. 15, no. 5, pp. 3311–3326, May 2016.

[16] X. Yu, J.-C. Shen, J. Zhang, and K. B. Letaief, "Alternating minimization algorithms for hybrid precoding in millimeter wave MIMO systems," *IEEE J. Sel. Topics Signal Process.*, vol. 10, no. 3, pp. 485–500, Apr. 2016.

[17] F. Khalid, "Hybrid beamforming for millimeter wave massive multiuser MIMO systems using regularized channel diagonalization," *IEEE Wireless Commun. Lett.*, vol. 8, no. 3, pp. 705–708, Jun. 2019.

[18] M. M. Molu, P. Xiao, M. Khalily, K. Cumanan, L. Zhang, and R. Tafazolli, "Low-complexity and robust hybrid beamforming design for multi-antenna communication systems," *IEEE Trans. Wireless Commun.*, vol. 17, no. 3, pp. 1445–1459, Mar. 2018.

[19] J. Li, L. Xiao, X. Xu, and S. Zhou, "Robust and low complexity hybrid beamforming for uplink multiuser mmWave MIMO systems," *IEEE Commun. Lett.*, vol. 20, no. 6, pp. 1140–1143, Jun. 2016.

[20] C.-K. Ho, H.-Y. Cheng, and Y.-H. Huang, "Hybrid precoding processor for millimeter wave MIMO communications," *IEEE Trans. Circuits Syst. II, Exp. Briefs*, vol. 66, no. 12, pp. 1992–1996, Dec. 2019.

[21] R. Mai, D. H. N. Nguyen, and T. Le-Ngoc, "MMSE hybrid precoder design for millimeter-wave massive MIMO systems," in *Proc. IEEE Wireless Commun. Netw. Conf.*, Apr. 2016, pp. 1–6.

[22] D. H. N. Nguyen, L. B. Le, T. Le-Ngoc, and R. W. Heath, Jr., "Hybrid MMSE precoding and combining designs for mmWave multiuser systems," *IEEE Access*, vol. 5, pp. 19167–19181, 2017.

[23] A. Morsali, A. Haghighat, and B. Champagne, "Realizing fully digital precoders in hybrid A/D architecture with minimum number of RF chains," *IEEE Commun. Lett.*, vol. 21, no. 10, pp. 2310–2313, Oct. 2017.

[24] A. Morsali, B. J. Champagne, and A. Haghighat, "Efficient implementation of hybrid beamforming," U.S. Patent App. 16 477 004, Nov. 21, 2019.

[25] A. Alkhateeb and R. W. Heath, Jr., "Frequency selective hybrid precoding for limited feedback millimeter wave systems," *IEEE Trans. Commun.*, vol. 64, no. 5, pp. 1801–1818, May 2016.

[26] F. Sohrabi and W. Yu, "Hybrid analog and digital beamforming for mmWave OFDM large-scale antenna arrays," *IEEE J. Sel. Areas Commun.*, vol. 35, no. 7, pp. 1432–1443, Jul. 2017.

[27] T. Lin, J. Cong, Y. Zhu, J. Zhang, and K. Ben Letaief, "Hybrid beamforming for millimeter wave systems using the MMSE criterion," *IEEE Trans. Commun.*, vol. 67, no. 5, pp. 3693–3708, May 2019.

[28] J. Du, W. Xu, H. Shen, X. Dong, and C. Zhao, "Hybrid precoding architecture for massive multiuser MIMO with dissipation: Sub-connected or fully connected structures?" *IEEE Trans. Wireless Commun.*, vol. 17, no. 8, pp. 5465–5479, Aug. 2018.

[29] R. Magueta, D. Castanheira, A. Silva, R. Dinis, and A. Gameiro, "Hybrid multi-user equalizer for massive MIMO millimeter-wave dynamic subconnected architecture," *IEEE Access*, vol. 7, pp. 79017–79029, 2019.

[30] C. E. Shannon, *The Theory and Design of Linear Differential Equation Machines*. Murray Hill, NJ, USA: Bell Labs, 1942.

[31] F. Bonchi, P. Sobociński, and F. Zanasi, "The calculus of signal flow diagrams I: Linear relations on streams," *Inf. Comput.*, vol. 252, pp. 2–29, Feb. 2017.

[32] D. M. Pozar, *Microwave Engineering*. Hoboken, NJ, USA: Wiley, 2005.

[33] E. Torkildson, U. Madhow, and M. Rodwell, "Indoor millimeter wave MIMO: Feasibility and performance," *IEEE Trans. Wireless Commun.*, vol. 10, no. 12, pp. 4150–4160, Dec. 2011.

**ALIREZA MORSALI** (Graduate Student Member, IEEE) received the B.Sc. and M.Sc. degrees in electrical engineering from Shahid Bahonar University, Kerman, Iran, in 2009, and 2011, respectively. He is currently pursuing the Ph.D. degree with McGill University, Montreal, QC, Canada. His research interests include coding theory, signal processing, wireless communications, and artificial intelligence. He was a recipient of several awards and scholarships, including, the McGill Engineering Doctoral Award, STARaCom Collaborative Grant, and McGill BLUE Fellowship.

**AFSHIN HAGHIGHAT** (Senior Member, IEEE) received the B.S. degree from the KNT University of Technology, Tehran, Iran, in 1992, and the M.A.Sc. and Ph.D. degrees from Concordia University, Montreal, QC, Canada, in 1998 and 2005, respectively, all in electrical engineering. He is currently a Principal Engineer with InterDigital, Inc., where he has been involved in advanced research and standardization of 5G NR and 4G LTE cellular systems. Prior to InterDigital, he was at Harris Corporation, from 1998 to 2005, where he contributed and led the development of advanced software-defined modems for high data rate backhaul point-to-point microwave systems. Before joining Harris, he worked at SR Telecom, from 1997 to 1998, where he was responsible for design and implementation of various microwave integrated transceiver platforms for point-to-multipoint radios. His main areas of interest and expertise are RF systems, communications, and signal processing.

**BENOIT CHAMPAGNE** (Senior Member, IEEE) received the B.Ing. degree in engineering physics from the Ecole Polytechnique of Montreal, in 1983, the M.Sc. degree in physics from the University of Montreal, in 1985, and the Ph.D. degree in electrical engineering from the University of Toronto, in 1990. From 1990 to 1999, he was an Assistant and then an Associate Professor with INRS Telecommunications, Montreal. In 1999, he joined McGill University, where he is currently a Full Professor with the ECE Department. His research interests include statistical signal processing and wireless communications, where he has coauthored more than 300 publications. He has been Associate Editor of the IEEE Signal Processing Letters and the IEEE Transaction on Signal Processing.